THE OPTICAL PROPERTIES OF A FAR INFRARED RADIOMETER

by

Frank James Wentz III

S.B., Massachusetts Institute of Technology

(1969)

SUBMITTED IN PARTIAL FULFILLMENT

OF THE REQUIREMENTS FOR THE

DEGREE OF MASTER OF

SCIENCE

at the

MASSACHUSETTS INSTITUTE OF TECHNOLOGY

November 1970 (i.e. Feb. 1971)

Signature of Author _____
Department of Physics
November 5, 1970

Certified by _____
Thesis Supervisor

Accepted by _____
Chairman, Departmental Committee
on Graduate Students

Archives

MASS. INST. TECH.
FEB 9 1971
LIBRARIES

ABSTRACT

THE OPTICAL PROPERTIES OF A FAR INFRARED RADIOMETER

Frank James Wentz III

Submitted to the Department of Physics on November 5, 1970 in partial fulfillment of the requirement for the degree of Master of Science.

A mock-up version of a balloon-borne far infrared radiometer flown by Muehlner and Weiss[1] was studied. The radiometer employed a conical horn to collect the radiation, and an InSb crystal served as a detector. The radiometer's angular response was measured for various situations.

It was found that the angular response of the conical horn could be closely represented by the geometric response with the addition of a weak tail at large angles to account for diffraction. Furthermore, the radiometer's angular response was shown to be considerably broadened by reflections off metallic apertures used in the radiometer. Finally, the angular distributions for the SR-2 and SR-3 arrangements used in the balloon-borne radiometer were measured and found not to differ significantly.

Thesis Supervisor: Rainer Weiss
Title: Associate Professor of Physics

CONTENTS

FIGURES

Chapter 1: Introduction

The experiment discussed in this thesis is an investigation of the optical properties of a far infrared radiometer. This radiometer was a mock-up version of a balloon-borne radiometer flown by Muehlner and Weiss[1] in 1969 to investigate the night sky brightness in the spectral region below 20 cm^{-1}. In the proposed flight for 1971, they will use a modified version of the same radiometer. The balloon-borne radiometer was completely immersed in liquid helium. It employed an aluminum cone to collect the radiation and an InSb crystal , located near the cone's apex, to detect the radiation. The major difference between this radiometer and the mock-up version was that in the latter the cone and detector were separated by a 15 in. light pipe and the cone was at room temperature.

The balloon-borne radiometer had a 1.75 in. dia. aperture at the large opening of the cone, and above this aperture was an objective lens. Above the lens was an area where filters were inserted into the path of the incident radiation by a solenoid driven cam mechanism. The purpose of the experiment to be discussed was to determine what effect the aperture, lens, and filters had on the angular response of the radiometer. This information would be useful in designing an improved version of the radiometer and in interpreting the data from the 1969 balloon experiment. To determine this effect, ten runs were made in which the angular response

of the radiometer was measured for different combinations of the aperture, lens, and filters. The measured angular response curves for some of the runs were compared with derived curves.

The derived curves were found by using geometric optics; that is, diffraction was not considered. These curves corresponded closely to the data except for large angles where the geometric response was zero. In this region the radiometer response was not zero although it was down by a large factor. Diffraction is one cause for this non-zero response. A solution that takes into account diffraction requires solving the boundary value problem for a multi-mode conical horn. The exact solution to this problem could not be found in the literature, and it was thought to be too complex to be solved in this thesis.

Chapter 2: The Source

To test the radiometer it was necessary to have a source of far infrared radiation. The source first used was a General Electric MV400 multivapor lamp which had the outside glass envelope removed thereby exposing the inner quartz bulb. The glass was removed because it absorbs infrared radiation. Later when this bulb burnt out, it was replaced by a mercury vapor lamp made in our glass shop. Both bulbs were operated near 400 watts using a 125 volt D.C. power supply in series with a current limiting resistor. After a one half hour warming up period, the emissions from the bulbs were very stable. Fluctuations with a period of a few seconds were measured to be less than 1%, and the drift in emission over several hours was less than 5%. These bulbs were chosen primarily for the large size of the arc which was about 5 cm long and .5 cm wide. The large arc has a large emitting surface thus producing a strong total emission. The emission was measured and found not to be constant over the cross section of the arc seen by the radiometer. It varied by about 15%, being strongest at the center of the arc.

The mechanism by which these bulbs radiate in the far infrared is discussed by Cano and Mattioli[2] and by Papoular[3]. The spectrum of emission can be divided into three regions: above $40cm^{-1}$ where emission from the quartz bulb is larger than the arc emission; between 20 cm^{-1} and 40 cm^{-1} where the arc emission behaves like that

from an optically thin plasma and competes with the quartz bulb emission; and below 20 cm^{-1} where the combined emission from the bulb and arc behaves like the emission from a black body near $3500^{\circ}K$. The radiometer is sensitive to radiation in this last region.

The Optics

Fig. 1 shows the optical setup for the experiment. A chopper was placed 1.5 in. from the source. It had eleven evenly spaced 1 in. dia. holes and was driven by a synchronous motor at 1800 rpm, thus chopping the light 330 times per second. The chopped light then passed thru a 1 in. dia. aperture and onto the field lens made of polyethylene with a dia. of 4 in. and a focal length of 6 in. The source was at the focal point of the field lens. A mirror was located 65.5 in. from the field lens. It consisted of a flat piece of aluminum mounted on a turntable, and could be rotated about an axis perpendicular to the incoming light while maintaining a constant 45° angle with respect to the axis of rotation. The axis of rotation coincided with the axis of the radiometer cone. The distance between the large opening of the cone, to be called the flare aperture, and the point where the cone axis intersected the mirror was 3 in. The incident angle θ that the reflected light made with the cone axis was then equal to the angle thru which the mirror had been rotated from $\theta = 0^{\circ}$. This proved to be the simplest arrangement because it avoided having to move either the source or the radiometer. The dimensions of the aluminum cone are shown

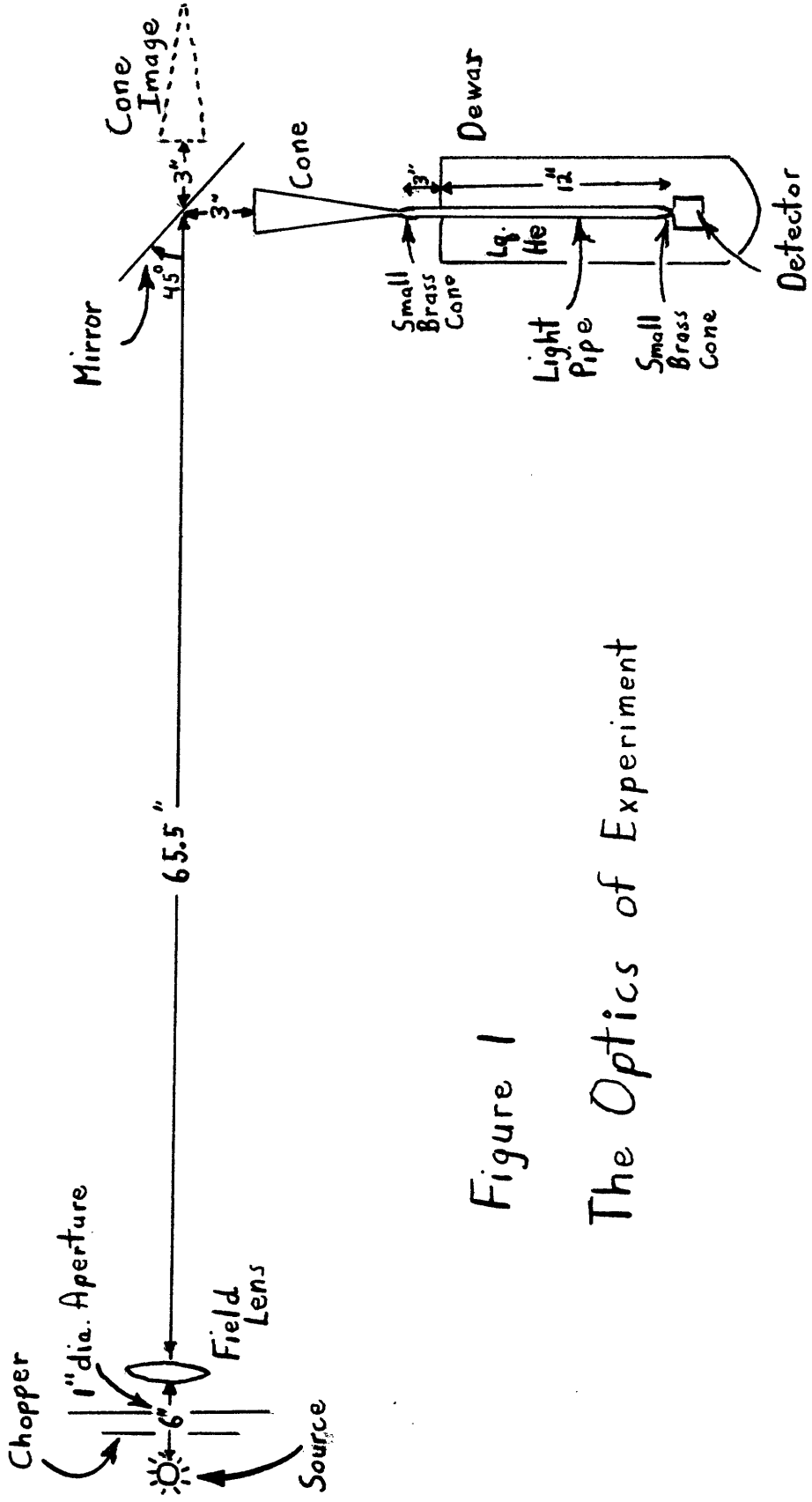

Figure 1

The Optics of Experiment

in Fig. 2. At the small end of the cone, called the apex aperture, was attached a small brass cone which flared out to fit a .5 in. dia. light pipe made of stainless steel with a gold-coated interior. The light pipe led down into a dewar of liquid helium at 4.2°K. Another small brass cone was attached to the bottom end of the light pipe. It tapered down to a .2 in. dia. opening which led into an aluminum cavity containing the infrared detector. Immediately in front of the detector was a 3/32 in. thick Fluorogold disk. The Fluorogold, a glass-filled Teflon, acted as a low-pass filter cutting off near 25 cm^{-1}, thereby isolating the region of interest.

The Detector

The detector, known as a "hot electron bolometer" or Rollin detector[4,5], consisted of a crystal of high purity n-type InSb. The crystal was cut to 5x7x½ mm size with gold leads soldered to the short ends. The preparation of these crystals is described by Muehlner[6]. In the crystal free electrons are loosely coupled to the crystal lattice and are at thermal equilibrium with the lattice in the absence of incident radiation. The absorption of radiation by the electrons raises their effective temperature and in this peculiar semiconductor increases their mobility. As a consequence InSb is a photoconductive radiation detector.

This type of detector was used for several reasons. First, it has its highest sensitivity, about 120 V/W, below 20 cm^{-1} which is the region of interest. Also it has a low noise equivalent

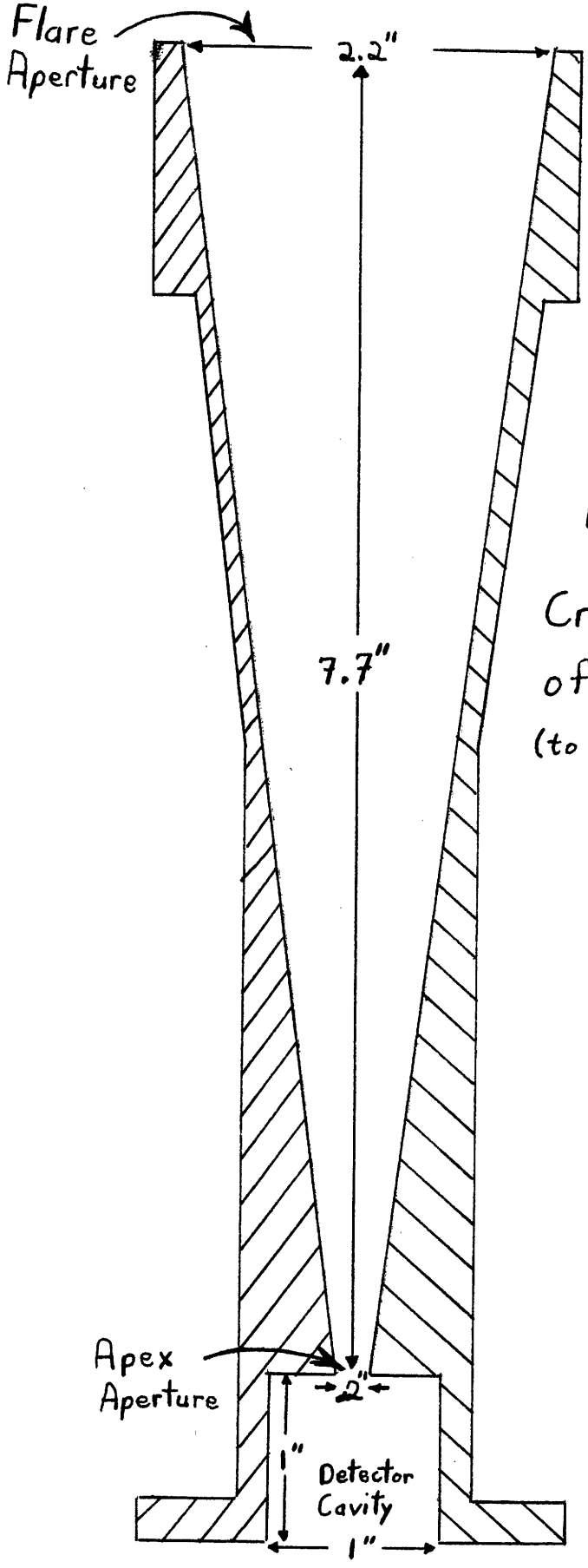

Figure 2

Cross Section of Cone (to scale)

power of about 10^{-12} W/Hz$^{\frac{1}{2}}$. Lastly, unlike bolometric detectors of the doped germanium types, it may be immersed in liquid helium. The detector used in this experiment was one of several tested. It was chosen because its sensitivity was the highest and its current noise was comparable, within a factor of two, to the Johnson noise at 4.2°K of a resistor of 100 ohms which is the resistance of the cold detector.

The Electronics

An impedance transformation was needed to match the low impedance detector to a high impedance, low noise preamplifier. A RLC circuit, shown in Fig. 3, which was resonant at 330 Hz, the chopping frequency, accomplished this. The Q of the circuit was measured to be 33, thus giving an impedance step-up of $Q^2 = 1089$. The Johnson noise of the cold detector is about .15 nV/Hz$^{\frac{1}{2}}$. The RLC curcuit increased this by a factor of Q to a value of 5 nV/Hz$^{\frac{1}{2}}$ at the input of the preamplifier. This was comparable to the input noise of the preamplifier which was measured to be 4 nV/Hz$^{\frac{1}{2}}$. The 2.6 H coil in the circuit was placed in the liquid helium to make the Q as high as possible. Its resistance at 4.2°K was 40 ohms. The coil was wound in opposite directions on two D-shaped nylon cores to reduce coupling with external magnetic fields, and was shielded by two layers of superconducting lead sheet. To reduce microphonics, the coil was suspended on a soft spring. Also in the liquid helium was a 1.2 K resistor which set the detector current at 1 ma. This was the detector current which was determined experimentally to give the highest detectivity.

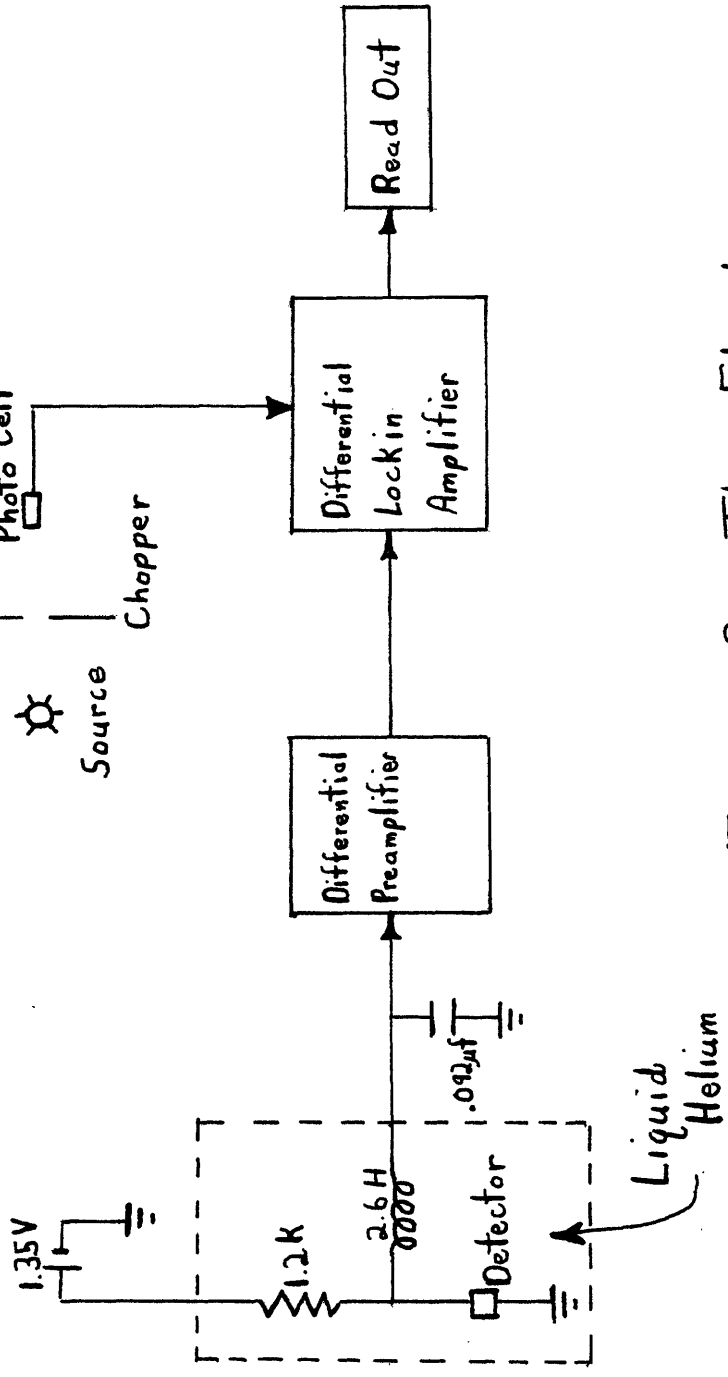

Figure 3. The Electronics

The rest of the electronics shown in Fig. 3 was outside the liquid helium. A 1.35 V Hg cell was the detector current source. The differential preamplifier had a low noise FET input stage, and integrated circuit operational amplifiers provided additional gain. The total gain was 4000. The preamplifier fed into a differential lock-in amplifier which employed a reference signal derived from a photocell that received the chopped light from the source. Most of the readings taken from the amplifier were for a one second time constant. For each run the reading was a maximum when light entered the cone at a 0° incident angle. Noise, coming mostly from microphonics in the coil, was measured to be a factor of two above the Johnson noise of the cold detector. The maximum signal to noise ratio is given in Table 1 for each run.

Chapter 3: Cone Channel Optics

The basic problem to be discussed in this and subsequent sections is to determine what fraction of light entering the flare aperture of the cone will pass thru the apex aperture. The assumption is made that the response of the radiometer is directly proportional to the intensity of light passing thru the apex aperture. The justification of this assumption is twofold. First, as discussed in Appendix 1, the transmission of the light pipe connecting the cone to the detector is only slightly dependent upon the incident angle of the light. The maximum variation in transmission as a function of incident angle was shown to be 2%. Secondly, the detector responds linearly to the intensity of radiation incident upon it. Therefore, to determine the angular response of the radiometer, one only needs to express the intensity of light passing thru the apex aperture as a function of the incident angle θ.

To begin the discussion on the optical properties of the cone, first consider the axial rays, those rays which intersect the cone axis at some point. Fig. 4 shows a simple ray tracing method described by Williamson[7] for determining which axial rays will pass thru the apex aperture. Any given axial ray can be traced by projecting the ray into image space and rotating the conical figure about the reflecting surface. This procedure is repeated for all subsequent reflections, thereby generating Fig. 4. Using this method it is a simple matter to determine

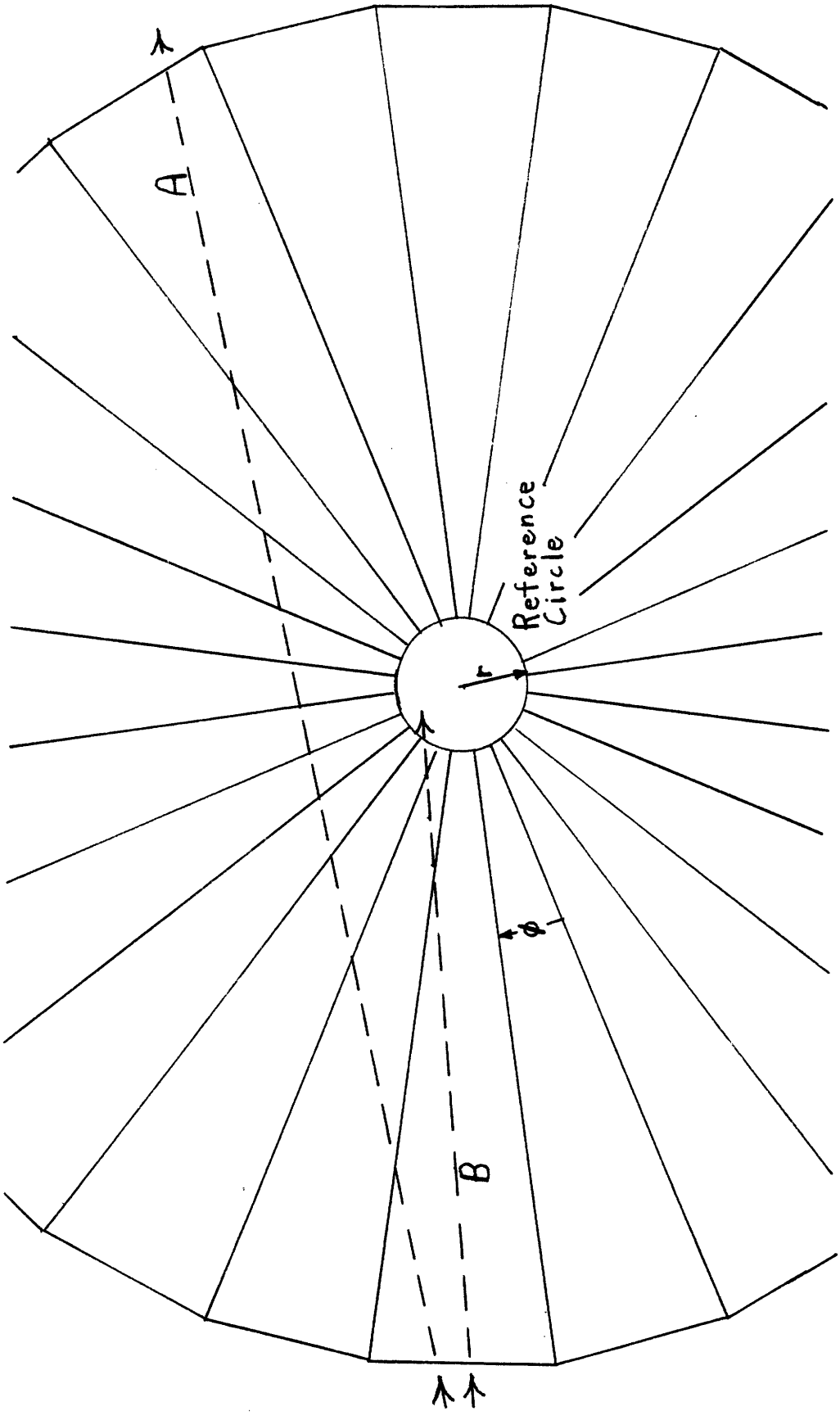

Figure 4 Cone Ray Tracing

that ray A will be reflected back out of the cone and ray B will pass thru the apex aperture. The polygon formed by the apex aperture can be approximated by a reference circle with radius $r = c/\sin\frac{\phi}{2}$, where c is the radius of the apex aperture and ϕ is the flare angle of the cone equaling 15°. For the cone used in this experiment r = .78 in. Any ray which intersects the reference circle passes thru the apex aperture, and all other rays are reflected back out of the cone.

In considering skew rays one must use a tridimensional ray tracing picture described by White[8]. The idea is basically the same as shown in Fig. 4 except that now a reference sphere is produced by the apex aperture when the cone is rotated about the reflecting surface. The reference sphere has the same radius as the reference circle, and as before all rays intersecting the reference sphere pass thru the apex aperture. Fig. 5 shows ray tracing done for the entire cross section of light entering the cone at incident angle θ. Plane M is perpendicular to the incident light and passes thru the reference sphere center. The area A represents the area of intersection of the reference sphere, the entering light, and plane M. The intensity of light passing thru the apex aperture is directly proportional to this overlap area A. The projection of light onto plane M is an ellipse with major axis equaling R, minor axis equaling $R\cos\theta$, and area equaling $\pi R^2\cos\theta$, where R is the radius of the flare aperture. In the following analysis θ will never exceed 16°, and therefore the ellipse can be nicely approximated by a circle of radius $R\cos^{\frac{1}{2}}\theta$, thereby

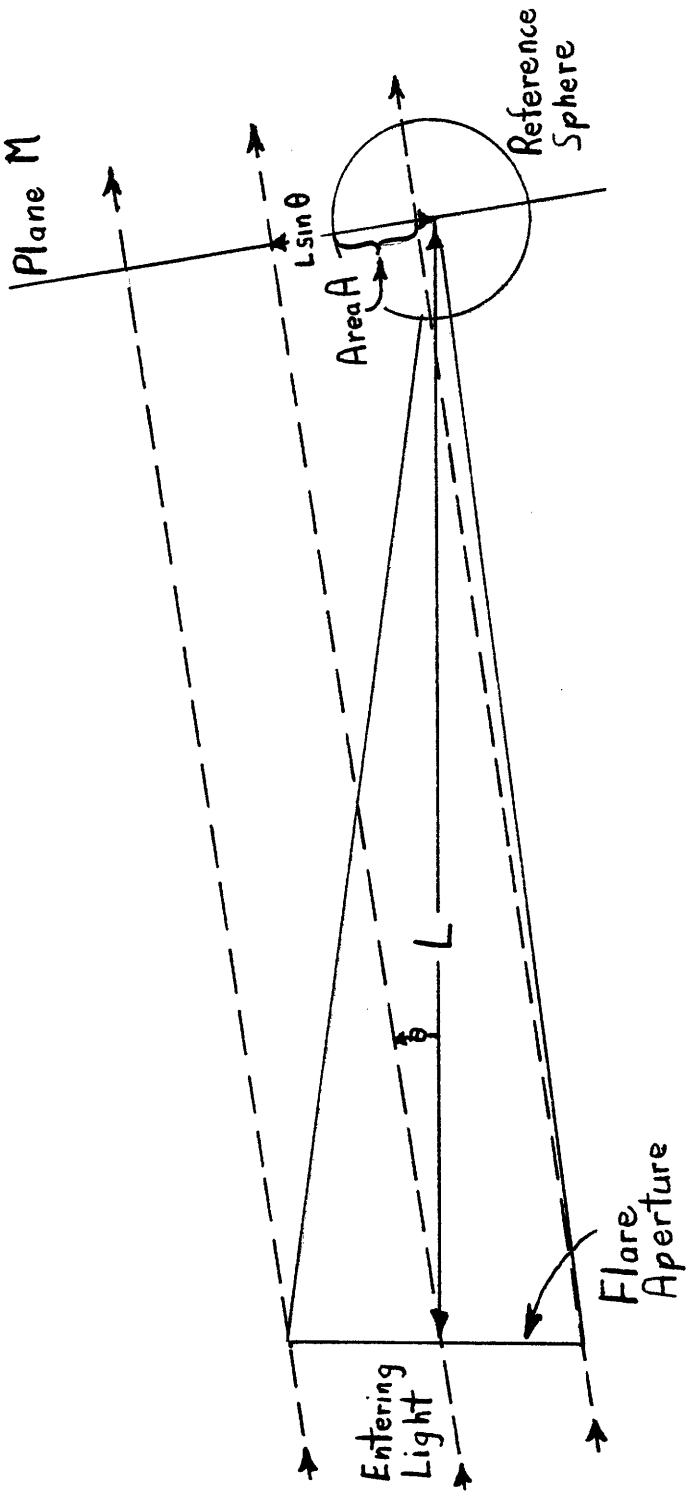

Figure 5 Ray Tracing for Skew Rays

making the areas of the ellipse and circle equal. With this approximation area A simply equals the overlap area of two circles of radius r and $R\cos^{\frac{1}{2}}\theta$, whose centers are separated by a distance $L\sin\theta$, where L is the distance from the flare aperture to the reference sphere center. In Appendix 2 area A is found as a function of θ. This function normalized to one for $\theta = 0^{\circ}$ is shown in Fig. 6 and indicates how the intensity of light I_o passing thru the apex aperture varies with θ. For $\theta > 12.7^{\circ}$ all the light is reflected back out of the cone. Note that $I_o(\theta)$ is the angular distribution for incident light which is parallel and of even illumination.

The Optics of the Source and Field Lens

In the experiment the light entering the cone was neither parallel nor of even illumination. In order to compare the geometric response of the cone with the experimental results, it is necessary to analyze the cone in conjunction with the source and field lens used in this experiment. For this analysis let the observation point be at the reference sphere center. Looking out of the cone towards the source, one sees the flare aperture and behind this the lens which acts as an aperture for light coming from the source image located at infinity. Refering back to Fig. 1 one finds that at the reference sphere center the flare aperture subtends a solid angle of .053 steradians; the lens, .0021 steradians; and the source image, .0218 steradians. The intensity of light at the observation point is proportional to the solid angle subtended by the visible portion of the source image which, in this case, equals the solid angle subtended by the lens. As the observation

Angular Distribution for Parallel, Uniform Light

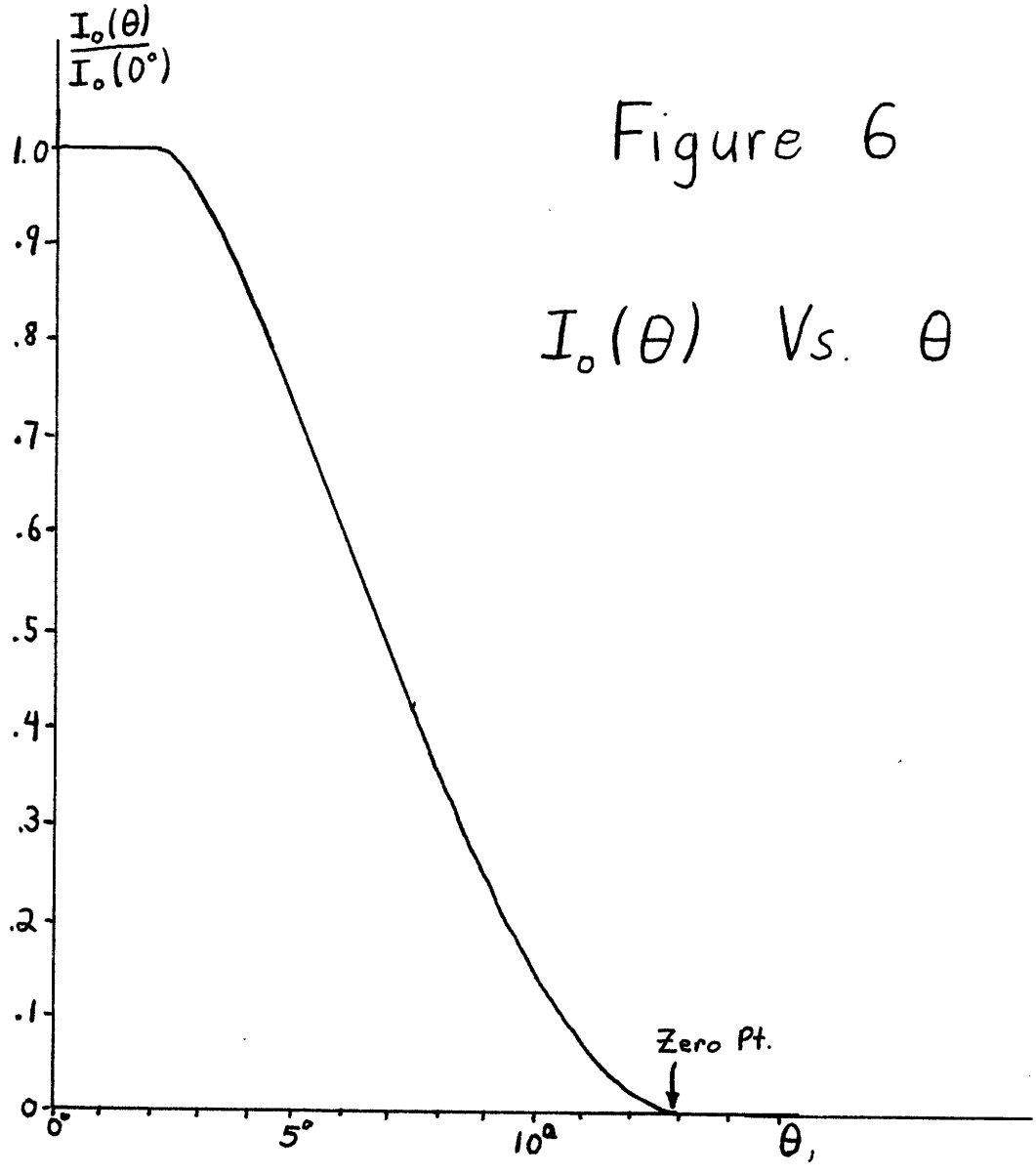

Figure 6

$I_o(\theta)$ Vs. θ

point is moved away from the reference sphere center along a line perpendicular to the cone axis, the intensity stays constant as long as the lens can be seen completely. At a distance of 1 in. from the center, the lens begins to become partially hidden by the flare aperture, and at a distance of 1.5 in. , it can not be seen at all. The solid angle subtended by the visible portion of the lens in the region between 1 in. and 1.5 in. can be expressed by the function derived in Appendix 2 for the overlap area of two circles where, in this case, the two circles are the lens and flare aperture. Let Ω represent the solid angle subtended by the visible portion of the source image, and let t represent the perpendicular distance from the cone axis at the reference sphere. Fig. 7 shows Ω as a function of t normalized to one at t = 0 as seen from the reference sphere. Note that $\Omega_o(t)$ can be closely approximated by

$$\Omega_o(t) = \begin{cases} 1 & t < 1 \\ 3-2t & 1 \le t \le 1.5 \\ 0 & t > 1.5 \end{cases} \quad \text{Eq. 1}$$

The source in this experiment did not provide even illumination. To determine the brightness distribution of the source, a .125 in. dia. aperture was placed over the flare aperture. The source and field lens were then moved along a line perpendicular to the axis of the cone's image in the mirror, keeping a constant incident angle of 0°. The small aperture was used so that all the light entering the cone would reach the reference sphere. Fig. 8 shows the situation where the lens and source have been moved a distance y from

Figure 7 Solid Angle Ω Vs. t

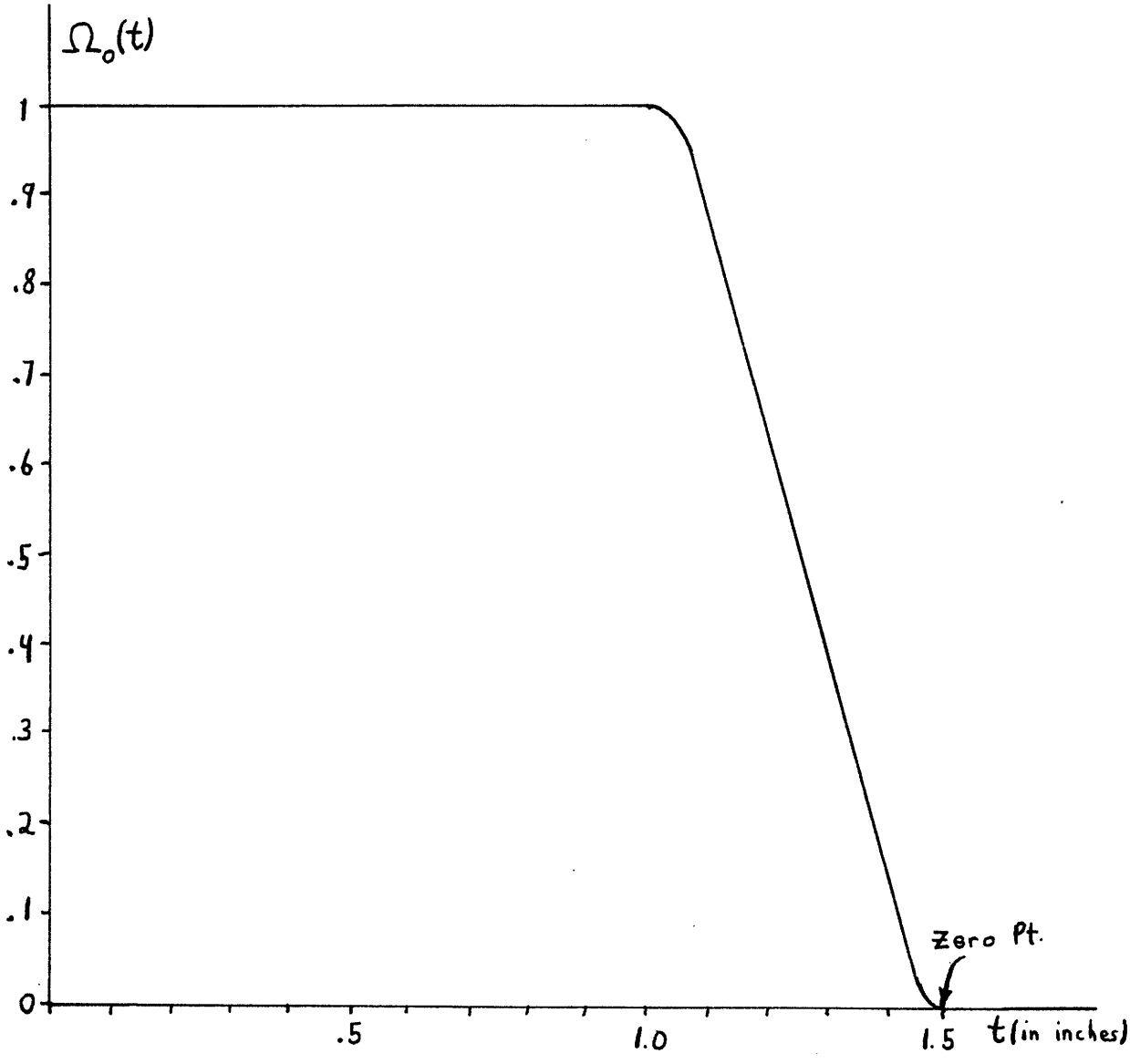

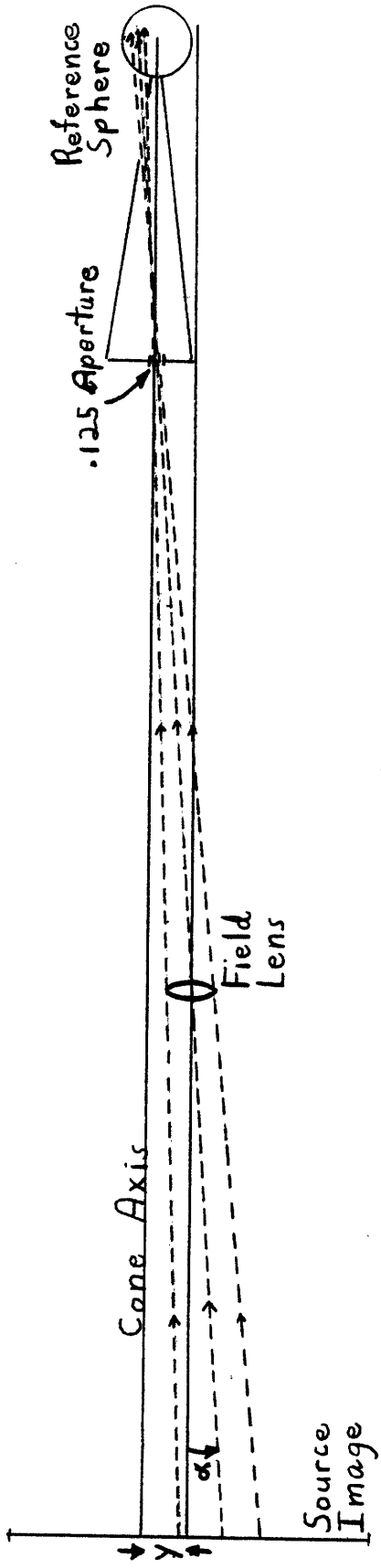

Figure 8 Experimental Arrangement for Finding $B'(\alpha)$

the axis of the cone's image. If the source image was of even illumination, the radiometer response would be unaffected when the source and lens were moved over small distances of a few inches or less. The response, however, does change, decreasing with increasing y. Since the total area of the source image which is visible at the reference sphere is constant, independent of y, this change in response is solely due to the uneven illumination of the source image. Fig. 9 shows the brightness of the source B' as a function of α, the angle shown in Fig. 8. The results indicate that $B'(\alpha)$ is approximately symmetric about the center of the source.

The intensity of light striking the reference sphere at a distance t from its center is proportional to the solid angle $\Omega_o(t)$ multiplied by the corresponding brightness B(t) of that solid angle. Refering to Fig. 10 one see that $\tan\alpha = t/77$, where t is always given in inches. Since t will not exceed a few inches, the approximation can be made that $\alpha \approx t/77$, and the following relation is obtained

$$B(t) = B'(t/77). \qquad Eq. 2$$

Fig. 11 shows the intensity distribution $I_o'(t)$ over the reference sphere for $\theta = 0^o$, where

$$I_o'(t) = B(t)\,\Omega_o(t). \qquad Eq. 3$$

To determine the total intensity reaching the reference sphere one must integrate $I_o'(t)$ over the reference sphere. The integral

Figure 9 Brightness Distribution

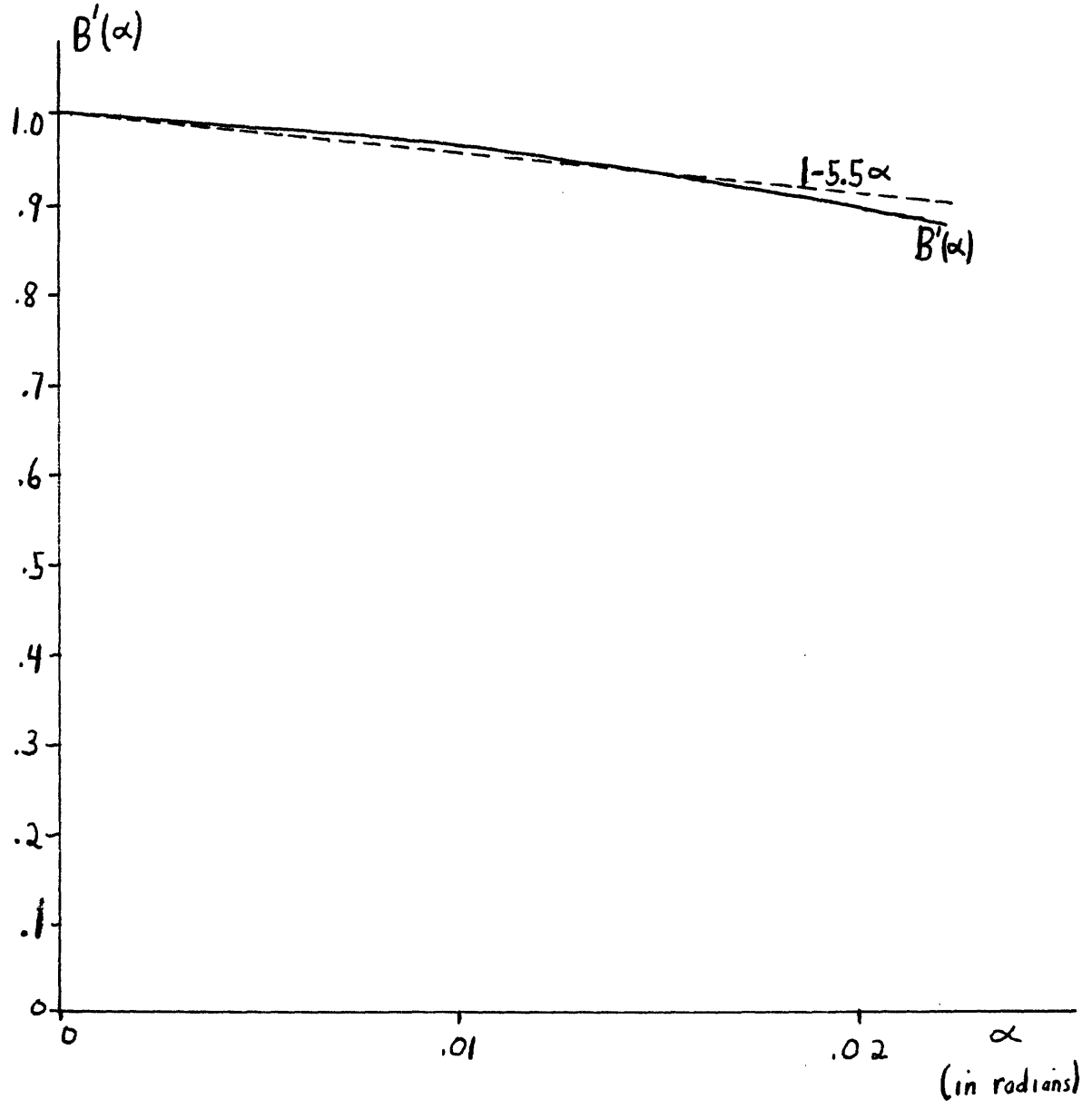

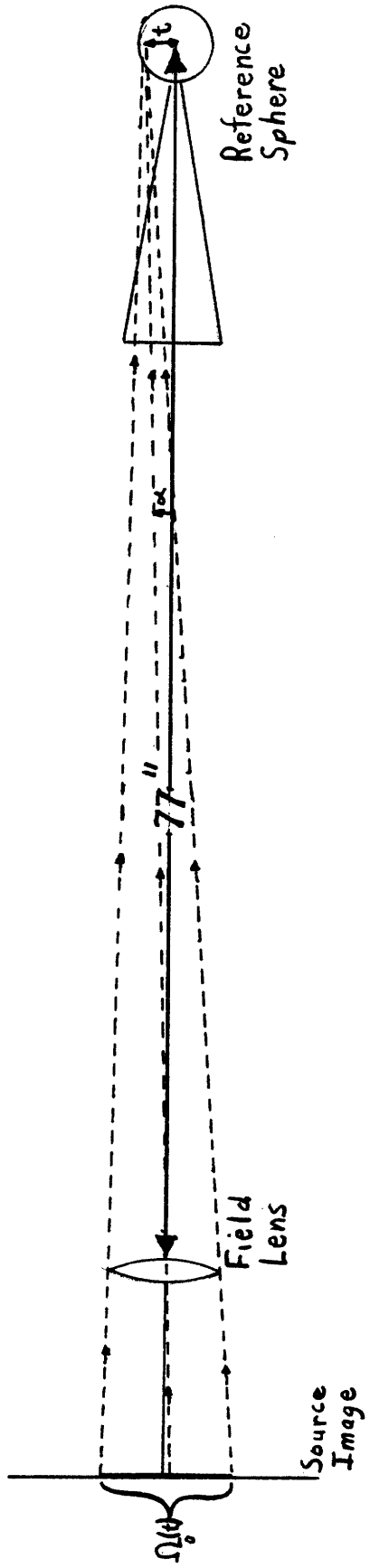

Figure 10 Calculation of $I_o'(t)$

Figure 11 $I_o'(t)$ Vs. t

Intensity of Light Over the Reference Sphere

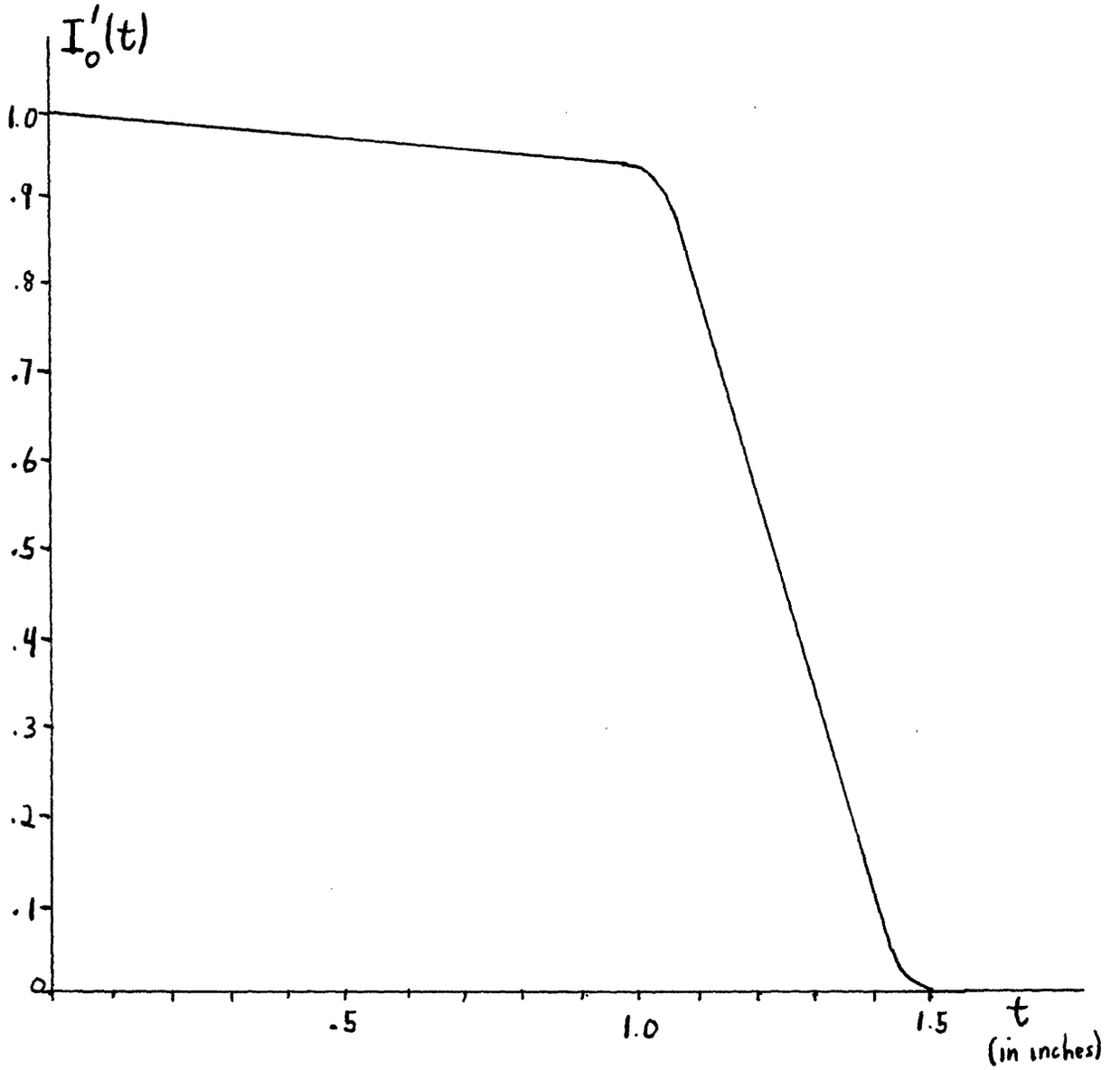

takes the form

$$I(0) = \int_0^r \Omega_0(t)\, B(t)\, 2\pi t\, dt \qquad \text{Eq. 4}$$

where r is as usual the radius of the reference sphere. Note that $\Omega_0(t) = 1$ over the entire range of integration. The total intensity I_t of light passing thru the flare aperture for $\theta = 0^\circ$ is given by the same integral except the integration is over all space. Thus I_t is given by

$$I_t = \int_0^\infty \Omega_0(t)\, B(t)\, 2\pi t\, dt \qquad \text{Eq. 5}$$

Doing these two integrals numerically one finds that

$$I_t / I(0) = 2.4 \qquad \text{Eq. 6}$$

Fig. 12 shows the cone image rotated about point B such that the incident angle of light equals θ. The $\theta = 0^\circ$ axis coincides with the cone image axis before it was rotated. The brightness distribution and solid angle Ω can no longer be represented solely as functions of the perpendicular distance from the cone axis. Since the flare aperture has be translated, the center P_1 of the cross section of light reaching the reference sphere is a distance $3.4 \sin\theta'$ from the $\theta = 0^\circ$ axis, where $\theta' = 1.05\theta$. It is, therefore, convenient to express Ω and the brightness distribution in a coordinate system whose origin is at P_1. Call this the prime system. Construct plane M, as before, normal to the incident light and containing the reference sphere center. Then the projection of light onto plane M is an ellipse with minor axis along line A and major axis perpendicular to A. It has already been determined that for

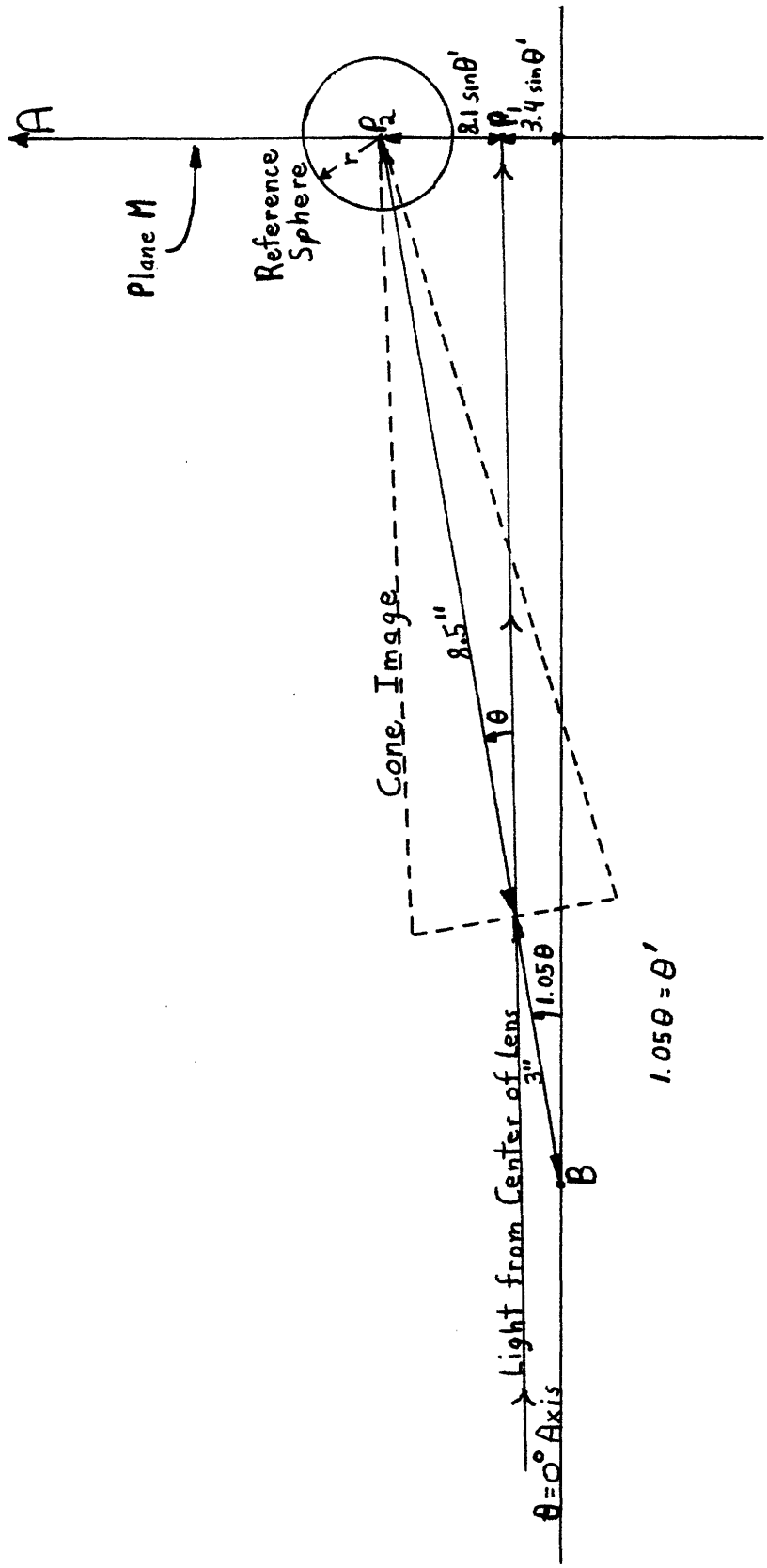

Fig. 12 Light Entering Cone at Incident Angle θ

$\theta = 0^{\circ}$ the ellipse becomes a circle with radius equaling the width of the solid angle distribution $\Omega_0(t)$, that being 1.5 in. Therefore, for non-zero θ, the resulting ellipse has a major axis equaling 1.5 in. and a minor axis equaling $1.5\cos\theta$ in. As before this can be closely approximated by a circle of radius equaling $1.5\cos^{\frac{1}{2}}\theta$ in. Let t' represent the radial distance measured in plane M from the origin of the prime coordinate system. Ω, when expressed as a function of t', has the same shape as shown in Fig. 7 except now its width equals the radius of the circle approximating the projection of light onto plane M. Therefore, Ω is given by

$$\Omega_\theta(t') = \Omega_0(t'/\cos^{\frac{1}{2}}\theta) . \qquad \text{Eq. 7}$$

To find the total intensity of light reaching the reference sphere, $\Omega_\theta(t')$ must be multiplied by the brightness distribution expressed in the prime coordinates. Then the product must be integrated over the reference sphere. Appendix 3 discusses approximations made so that the brightness distribution could be expressed as a function of t', and gives the details of the integration over the reference sphere. The final result $I(\theta)$, the total intensity of light passing thru the apex aperture for the specific source and field lens used in this experiment, is shown in Fig. 13.

The Aperture

The balloon-borne radiometer had a 1.75 in. dia. aperture at the flare aperture of the cone. To investigate its effect, several runs were made using such an aperture. Placing a brass aperture at

Figure 13

Intensity of Light at Apex Aperture Vs. θ
for Cone Alone and for Apertured Cone

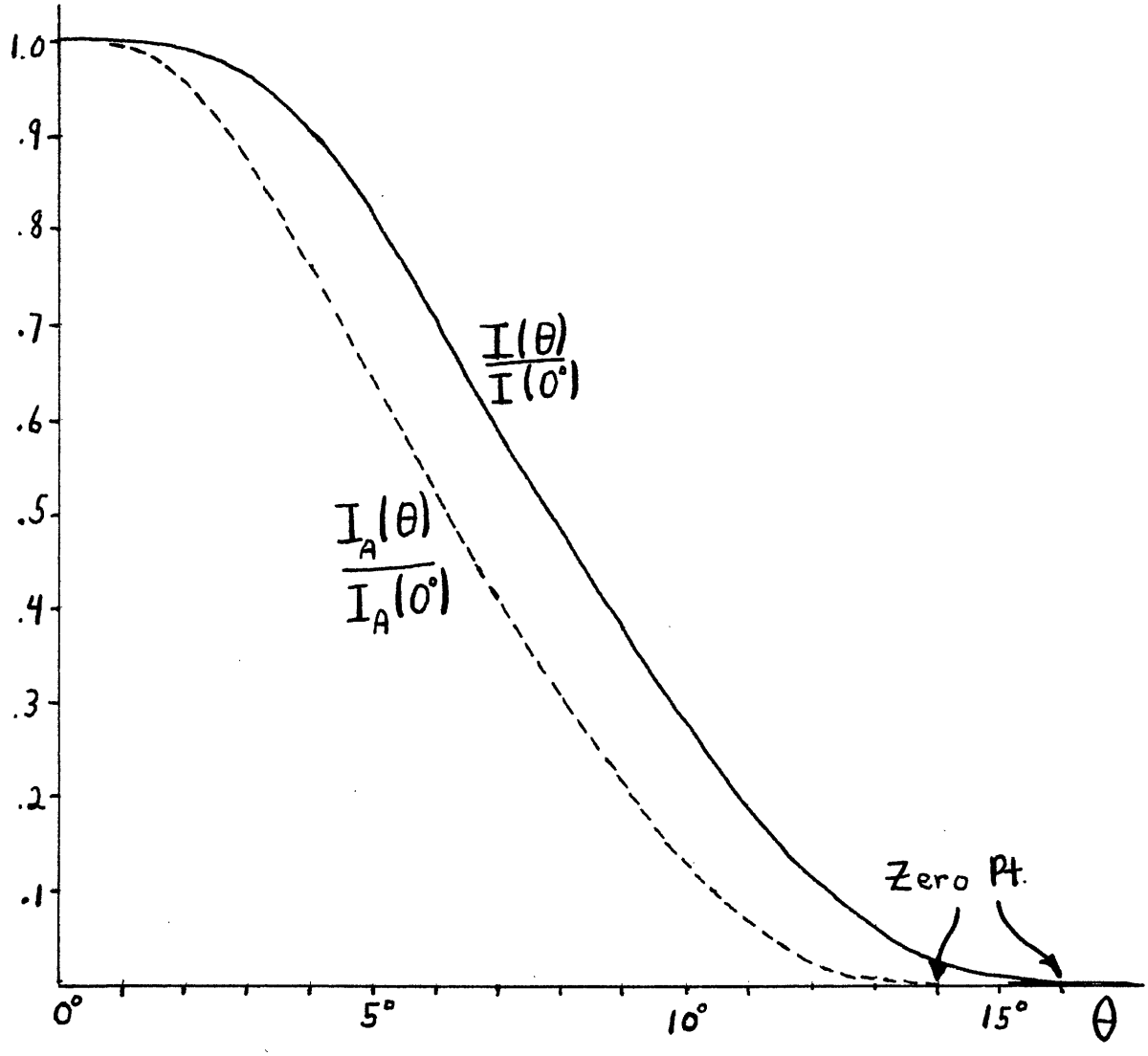

the flare aperture changes the function for Ω. Let $\Omega_o^A(t)$ represent Ω as a function of t for $\theta = 0^\circ$ when the brass aperture is present. $\Omega_o^A(t)$ can be found in the same manner as $\Omega_o(t)$, noting that in the calculation, the radius of the flare aperture is replaced by the radius of the brass aperture, this being .875 in. Doing this one finds

$$\Omega_o^A(t) = \Omega_o(1.25t) \qquad \text{Eq. 8}$$

where 1.25 is the ratio of the flare aperture radius to the brass aperture radius. Let $I_A(\theta)$ represent the intensity of light passing thru the apex aperture when the brass aperture is present. $I_A(\theta)$ is found in the same manner as was $I(\theta)$ except that $\Omega_o(t)$ is replaced by $\Omega_o^A(t)$ everywhere in the calculation. $I_A(\theta)$ is shown in Fig. 13. Note that

$$\begin{aligned} I_A(0) &= \int_0^r \Omega_o^A(t)\, B(t)\, 2\pi t\, dt \\ &= \int_0^r \Omega_o(t)\, B(t)\, 2\pi t\, dt \\ &= I(0) \end{aligned} \qquad \text{Eq. 9}$$

since both $\Omega_o(t)$ and $\Omega_o^A(t)$ equal one over the range of integration. Therefore, the brass aperture should have no effect on the $\theta = 0^\circ$ response of the radiometer.

The angular distribution $I_A(\theta)$ will be altered by reflections off the aperture. Some of the light which was reflected out of the cone will reflect off the aperture and re-enter the cone. The light is given a second chance to reach the reference sphere. Fig. 14 is a ray tracing disgram employing the same concepts as in Fig. 4

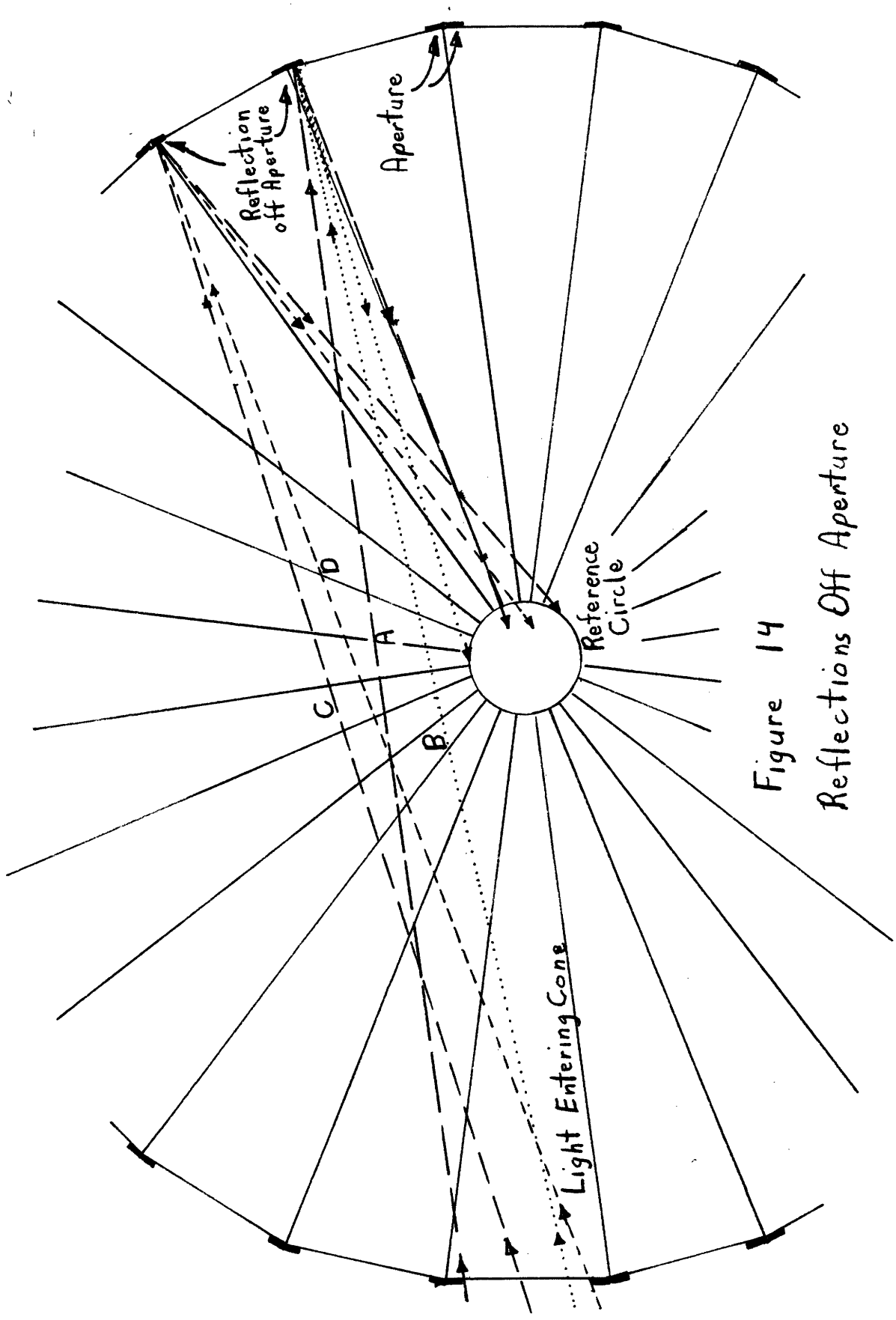

Figure 14
Reflections Off Aperture

except that the aperture has been included. It was found that for $8^\circ < \theta < 12.5^\circ$ and $18^\circ < \theta < 21^\circ$ part of the re-entering light reaches the reference sphere. For all other θ the re-entering light misses the reference sphere on the second try. The rays shown in Fig. 14 are extreme rays which reach the reference sphere. Ray A has an incident angle of 8°; ray B, of 12.5°; ray C, of 18°; and ray D, of 21°. The possibility of multiple reflections off the aperture occurring before the light enters the reference sphere was not taken into account because such an effect was considered to be insignificant. For incident angles lying in the two ranges stated above, there will be an enhancement of light entering the reference sphere which was not considered in the calculation of $I_A(\theta)$. Therefore, the response of the radiometer should be greater than $I_A(\theta)$ predicts for these two regions.

The Objective Lens

The balloon-borne radiometer employed an objective lens to sharpen the angular distribution. The plano-convex lens was made of Teflon, had a radius of curvature of 3.7 in., and had a focal length of 9.2 in. The lens was used in several runs so that its properties could be investigated. When the lens is placed over the flare aperture, a real image of the source image is formed near the reference sphere. The diameter of this image is about .5 in. Finding $I_L(\theta)$, the intensity of light passing thru the apex aperture when the lens is present, is simplified because the image is much smaller than the reference sphere. The brightness of the image can be nicely represented by the average of the

brightness distribution over the objective lens. Let $B_L(\theta)$ represent this average. Refering to Fig. 9 and Eq. 2, one finds a good approximation for the brightness distribution at the reference sphere is

$$B(z) = 1 - .08\,z \qquad \text{Eq. 10}$$

where z is the perpendicular distance from the $\theta = 0^\circ$ axis in Fig. 12. The brightness distribution as a function of z only changes slightly when the observation point is moved from the reference sphere to the flare aperture. Therefore the expression for B(z) in Eq. 10 can also be used to represent the brightness distribution at the flare aperture. Refering to Fig. 12, $B_L(\theta)$ can be written as

$$\begin{aligned} B_L(\theta) &= \int_{Lens} B(z)\,dA \Big/ \pi R^2 \\ &\approx \int_{3\sin\theta' - R\cos\theta'}^{3\sin\theta' + R\cos\theta'} (1 - .08z)\,dz \Big/ 2R\cos\theta' \\ &= 1 - .04(9\sin^2\theta' + R^2\cos^2\theta')/R\cos\theta' \qquad \text{Eq. 11} \end{aligned}$$

where the approximation for $B_L(\theta)$ is within 1% of its actual value.

For $\theta < 3.8^\circ$, the .5 in. dia. image and the reference sphere completely overlap and thus $I_L(\theta)$ is simply proportional to $B_L(\theta)$. For $\theta > 7.3^\circ$, the image and the reference sphere do not intersect and $I_L(\theta) = 0$. For the in between region the image and the reference sphere partially overlap. To calculate $I_L(\theta)$ in this region requires knowing the intensity distribution across the image. The intensity distribution is very sensitive to the distance between

the lens and where the image intersects the reference sphere, and for this reason it was not determined exactly. The approximation was made that the intensity was constant over the image. With this approximation $I_L(\theta)$ is simply proportional to the overlap area of the image and the reference sphere times $B_L(\theta)$. The function for the overlap area is given in Appendix 2. $I_L(\theta)$ is shown in Fig. 15.

For $\theta = 0^\circ$ all the light passing thru the flare aperture is focused onto the reference sphere. The total intensity of light passing thru the flare aperture is given by Eq. 5. Since $I_t = I_L(0)$ one has from Eq. 6

$$I_L(0)/I(0) = 2.4 \qquad \text{Eq. 12}$$

The Filters

Several runs were made in which the filters used in the balloon-borne radiometer were investigated. These filters were capacitive-grid, low-pass interference filters described by Ulrich[9]. In making these filters, silver was evaporated thru a wire mesh onto pieces of polyethylene, thus producing an array of metallic squares. Four such pieces were then fused together, making one filter. The size of the squares and the spacing of the polyethylene pieces determined the cutoff frequency of the filters. In this experiment filter A cut off at 8 cm^{-1}, filter B cut off at 12 cm^{-1}, and filter C, consisting of two filters placed in series, cut off at 10 cm^{-1}. The filters should reduce the $\theta = 0^\circ$ response of the radiometer. This reduction should vary inversely as the cube of the cutoff frequency because the intensity of the source goes as the square of the frequency in the region of interest.

Figure 15

Intensity of Light at Apex Aperture for Lens

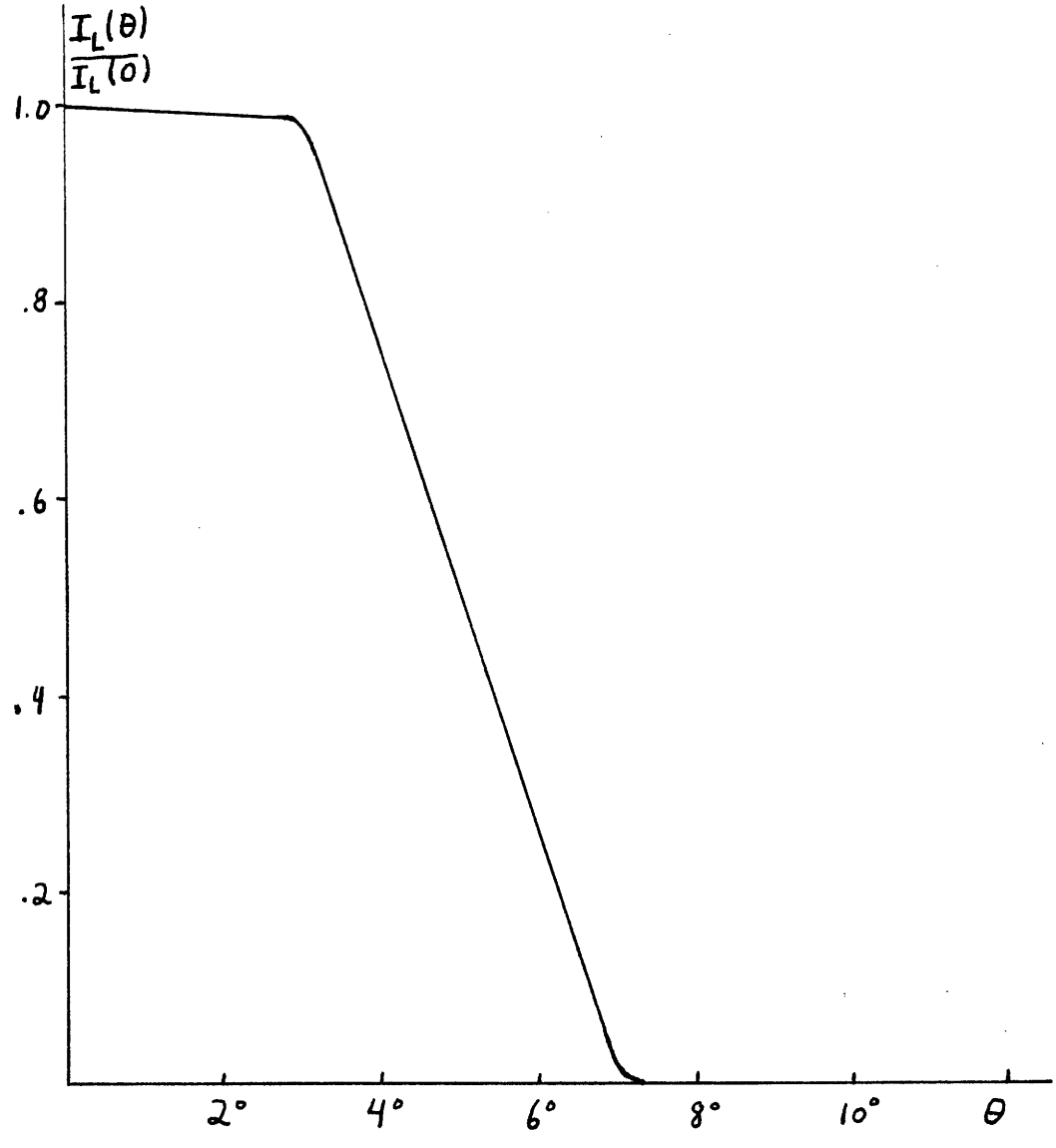

Diffraction

To determine if geometric optics provide an accurate model for the optics of the cone, the diffraction properties of the cone must be considered. To solve exactly for the diffraction in a cone involves solving Maxwell's equations in a conical horn with the appropriate boundary conditions imposed at the flare aperture to account for the incident radiation. Schorr and Beck[10] did this for low order modes by an approximation method for cones with a flare aperture diameter D comparable to the wavelength λ of the observed radiation. Fig. 16 shows the angular distribution of a cone with a flare angle of 10° and $D/\lambda = 4$. This distribution differs considerably from that shown in Fig. 6 for geometric optics. In this experiment D/λ was greater than 25 for 95% of the measured radiation. For ratios this large there exist a large number of possible modes, and the approximation method of Schoor and Beck cannot be used. All that can be said is that the distribution shown in Fig. 16 becomes much sharper for larger D/λ .

The most important parameter affecting diffraction is the size of the flare aperture, not the apex aperture. As radiation goes down the cone, the cone's cross section decreases which results in greater spreading of the light due to diffraction. However, the increased spreading is offset by the fact that it occurs closer to the reference sphere. With this in mind, diffraction by the cone was considered to be solely a result of diffraction from the flare aperture. This diffraction would spread out the light passing thru the flare aperture, thus slightly broadening $\Omega_o(t)$. $\Omega_o(t)$

Figure 16

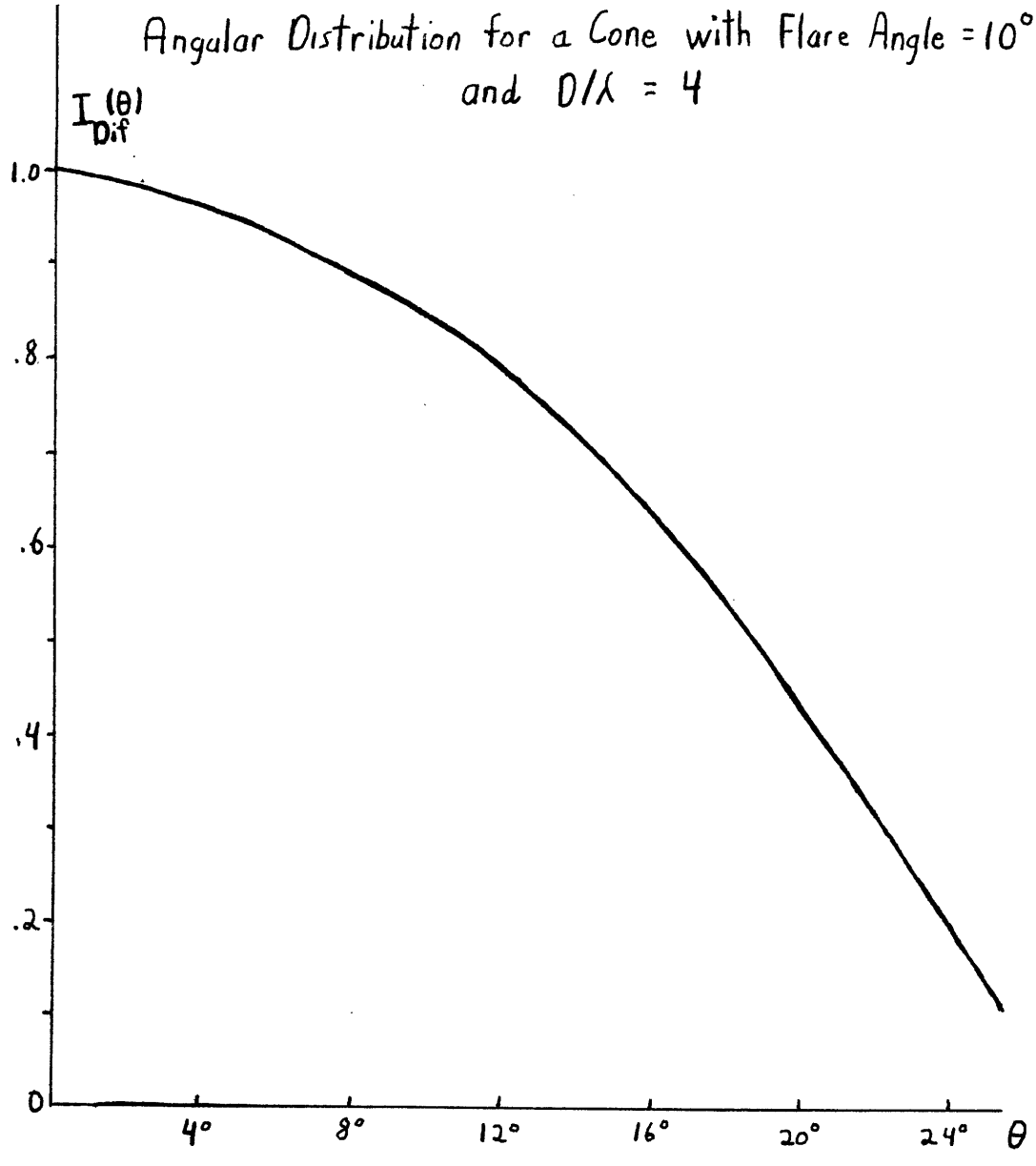
Angular Distribution for a Cone with Flare Angle = 10°
and D/λ = 4
$I_{Dif}(\theta)$
1.0
.8
.6
.4
.2
0
4°
8°
12°
16°
20°
24°
θ

would no longer be zero for $t > 1.5$ in. although its value in this region would be of the order of 10^{-5} or less. Therefore, a small portion of the entering light would still reach the apex aperture for angles where geometric optics perdict a zero response. However, the intensity for these large angles would be down by at least a factor of 10^{-5} from the $\theta = 0^{\circ}$ response.

Chapter 4: The Results

The response of the radiometer was measured as a function of incident angle for various combinations of filters, objective lens, brass aperture, and polyethylene cover. Table 1 lists the combination used in each run. The mirror used to vary the incident angle could be turned both clockwise and counterclockwise from the $\theta = 0^{\circ}$ setting, thereby providing two readings for each value of θ. Let $V_n'(\theta)$ be the radiometer response for an incident angle θ in the n^{th} run. The ratio $V_n'(0)/V_2'(0)$ is given in Table 1 for each run. Let $V_n(\theta)$ stand for the response $V_n'(\theta)$ which has been normalized to one at $\theta = 0^{\circ}$.

In Run 1 nothing was placed over the flare aperture. The circles in Fig. 17 indicate $V_1(\theta)$, and the error brackets for large angles indicate the uncertainty caused by noise. The solid curve is the calculated function $I(\theta)$. For $\theta < 16^{\circ}$, $I(\theta)$ and $V_1(\theta)$ compare nicely although $I(\theta)$ is a somewhat broader distribution. For $\theta > 16^{\circ}$, where $I(\theta)$ is zero, $V_1(\theta)$ is not zero. When the field lens was covered by a sheet of metal, the signal did go to zero thereby indicating that the non-zero response for large angles was due to radiation coming from the source. It would appear that the geometric analysis used to derive $I(\theta)$ does not provide an accurate picture for large angles, and that diffraction does have a measurable effect on the angular distribution. Note that $I(\theta)$ is dependent upon the source described by $B(t)$ and $\Omega_o(t)$ and upon the intrinsic properties of the cone. $B(t)$ is solely a property of the source, independent of diffraction effects. Furthermore, as discussed in the last section, $\Omega_o(t)$ is only slightly changed by diffraction occurring at the

Table 1

Run	Poly. Cover	Rough Interior	Aperture	Lens	Filter	$\frac{V_n'(0)}{V_n'(0)}$	Refer to	Max. Signal to noise ratio
1	NO	NO	NO	NO	NO	1.07	o Figs. 17 & 18	2×10^4
2	YES	NO	NO	NO	NO	1.00	+ Fig. 18	2×10^4
3	YES	YES	NO	NO	NO	1.00	x Fig. 18	2×10^4
4	YES	YES	NO	YES	NO	2.10	o Fig. 19	4×10^4
5	YES	YES	YES	NO	NO	1.00	+ Fig. 20	2×10^4
6	YES	YES	YES	YES	NO	1.85	o Fig. 21	4×10^4
7	YES	NO	YES blacken	YES	NO	1.85	+ Fig. 21	4×10^4
8	YES	YES	YES	YES	A	0.15	o Fig. 22	3×10^3
9	YES	YES	YES	YES	B	0.31	x Fig. 22	6×10^3
10	YES	YES	YES	YES	C	0.12	+ Fig. 22	3×10^3

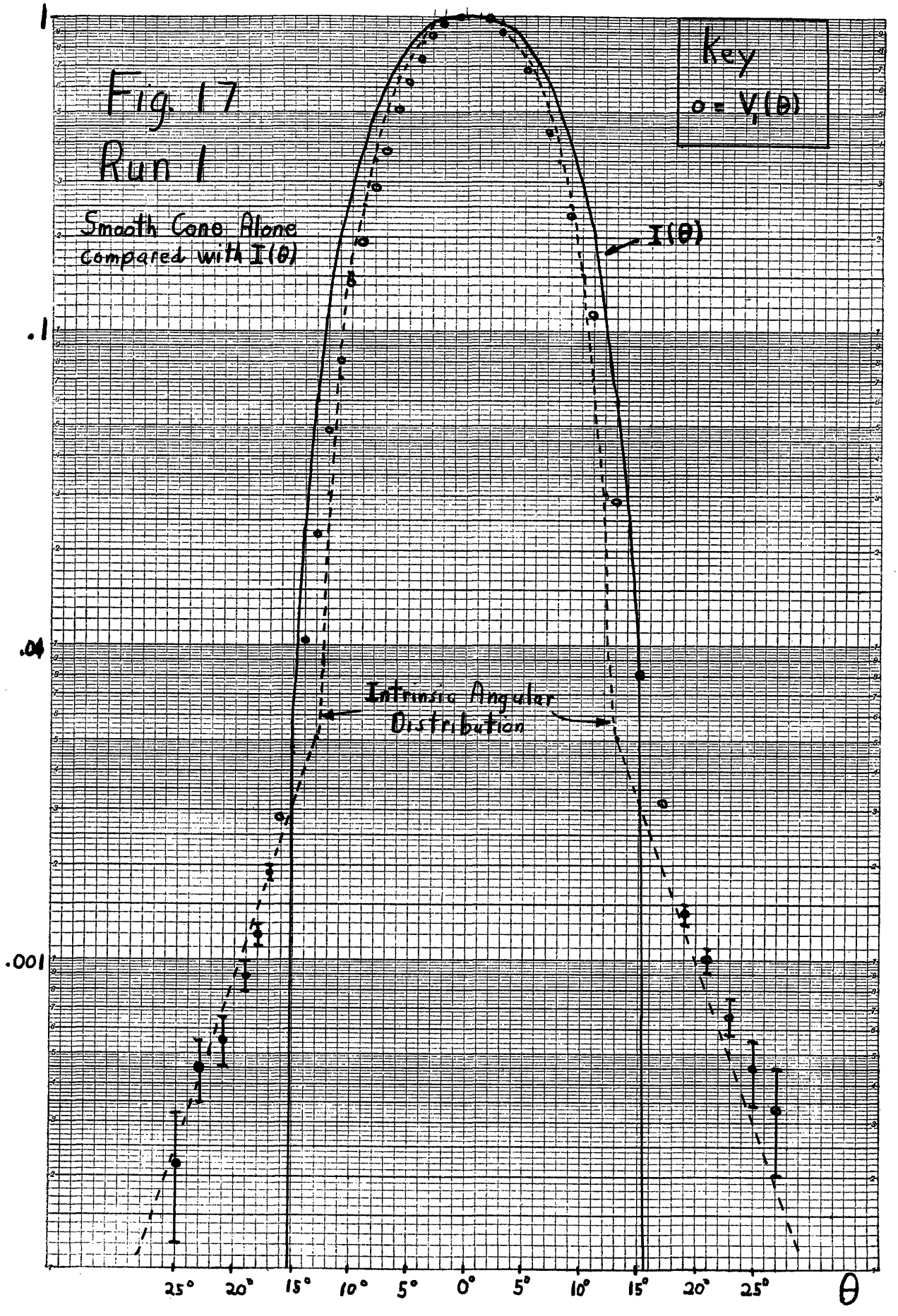
Fig. 17
Run 1
Smooth Cone Alone
Compared with I(θ)
Key
o = V_i(θ)
I(θ)
Intrinsic Angular
Distribution
1
.1
.01
.001
25°
20°
15°
10°
5°
0°
5°
10°
15°
20°
25°
θ

flare aperture. This slight change cannot explain $V_1(\theta)$ being so large for large angles. Therefore, the non-zero response must be an intrinsic property of the cone and not a property of the particular source used. From Fig. 17 it appears that the angular response of the cone can be nicely represented by the geometric response with the addition of a tail at large angles resulting from diffraction. The tail in Fig. 17 begins where the geometric response goes to zero with a value of .005 of the $\theta = 0^\circ$ response, and falls off by a factor of 10 over 10°. By adding such a tail to $I_o(\theta)$ in Fig. 6, one obtains a very good approximation of the angular response of the cone, independent of the particular source used in this experiment. This intrinsic angular distribution is shown in Fig. 17 by the broken curve.

In all subsequent runs a 2 mil polyethylene cover was placed over the flare aperture. The effect of this cover is shown in Fig. 18 where the crosses indicate $V_2(\theta)$, the response when the flare aperture was covered only by the polyethylene. The circles in Fig. 18 represent $V_1(\theta)$. The response for $\theta = 0^\circ$ decreased by 7% when the covered was placed over the cone. This decrease is what one expects from the reflection properties of a thin piece of polyethylene. There are no significant discrepancies in the data for Run 1 and Run 2 until the response fall below 1%. At this point $V_2(\theta)$ begins falling off slower than $V_1(\theta)$. It is believed that this is a result of light being reflected back into the cone by the cover, thus having a second chance to reach the apex aperture.

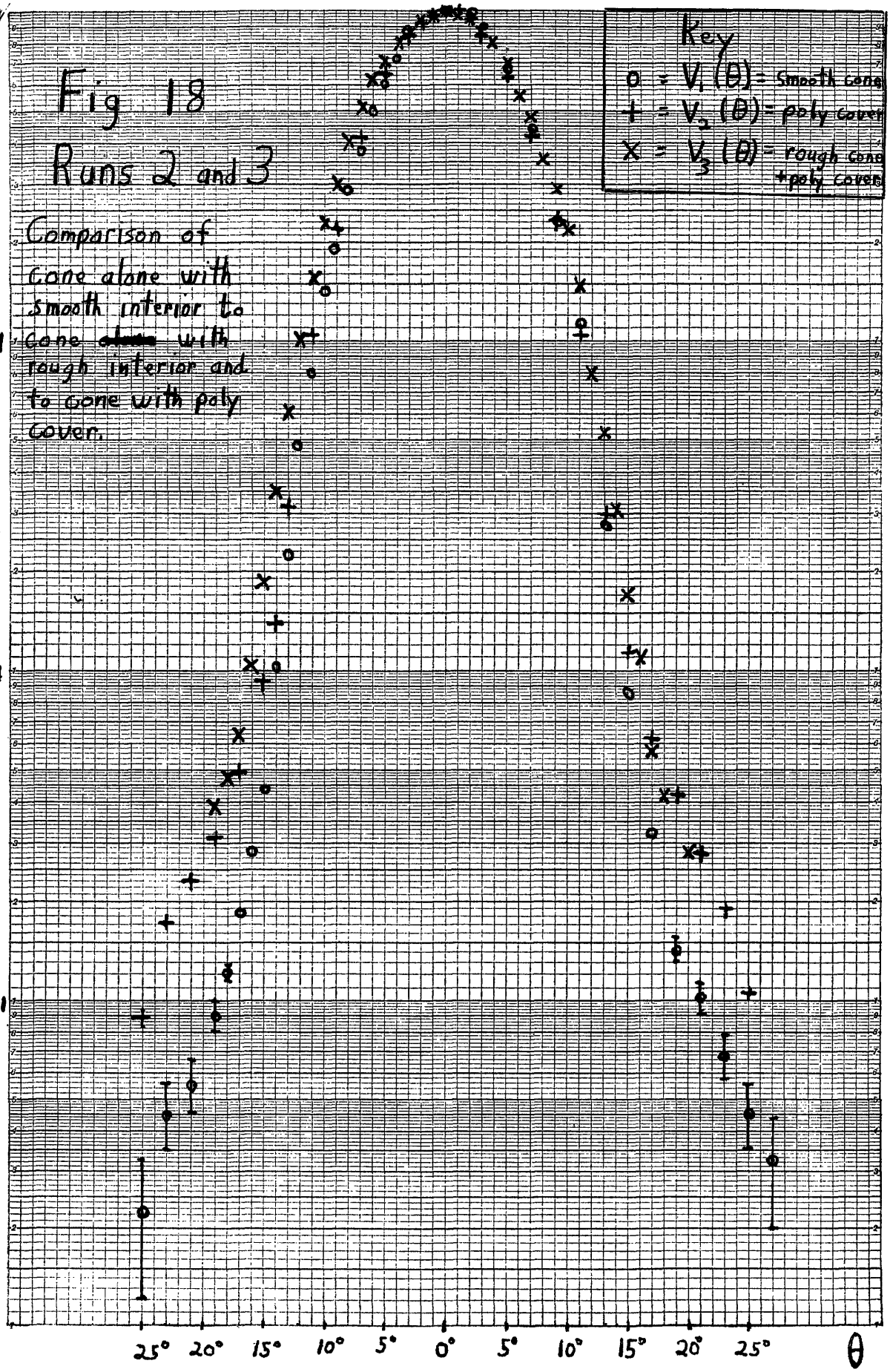
Fig 18
Runs 2 and 3
Comparison of Cone alone with smooth interior to Cone with rough interior and to Cone with poly cover.
Key
o = $V_1(\theta)$ = Smooth Cone
+ = $V_2(\theta)$ = poly Cover
x = $V_3(\theta)$ = rough Cone + poly Cover
1
.1
.01
.001
25° 20° 15° 10° 5° 0° 5° 10° 15° 20° 25°
θ

In Run 3 a second cone was used. The goemetry of the second cone was identical to the first; however, the second cone had circular grooves about 1 mil deep on the interior surface, whereas the first cone's interior was polished. The "x's" in Fig. 18 show $V_3(\theta)$. There is no significant difference in the data for Run 2 and Run 3. It appears that the effect of scattering from the rough surface is too small to measure.

An objective lens described previously was placed over the flare aperture in Run 4. $V_4'(0)/V_2'(0)$ was 2.1 whereas Eq. 12 predicts that this ratio should equal 2.4. The reflection properties of the lens will make this ratio less than predicted. The reflection from the surface of the lens is given by $(n-1)^2/(n+1)^2$, where n is the index of refraction of Teflon. Because the reflection is small and there are two surfaces, the total reflection by the lens is twice the above quantity. From this it was found that the transmission of the lens was .94 which reduces the perdicted ratio to 2.25 which is within 7% of the measured ratio. For $\theta = 2^\circ$ the lens was turned upside down so that the flat side of the lens was away from the flare aperture. This resulted in a 5% increase in signal, thus indicating that there is an asymmetry in the reflection or focusing properties of the lens. $V_4(\theta)$ is shown as circles in Fig. 19. The solid curve in Fig. 19 is the calculated function $I_L(\theta)$. The data corresponds closely to the predicted values up to 6°. At this point the experimental distribution begins to broaden in a manner similar to the data for Run 2. This is attributed again to light being reflected back into the cone by the polyethylene cover and the lens.

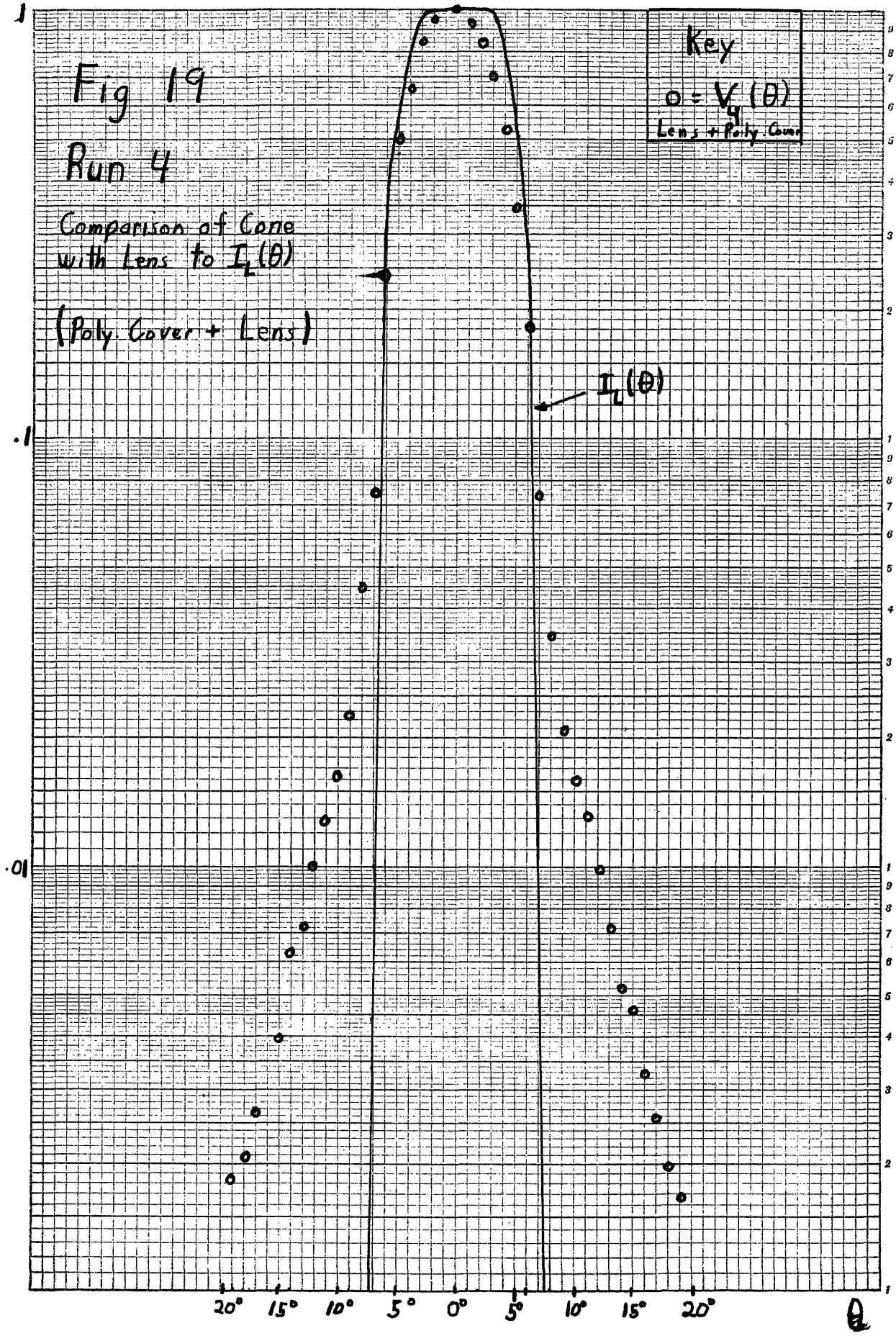
Fig 19
Run 4
Comparison of Cone with Lens to $I_L(\theta)$
(Poly. Cover + Lens)
Key
o = $V_4(\theta)$
Lens + Poly. Cover
$I_L(\theta)$
1
.1
.01
20° 15° 10° 5° 0° 5° 10° 15° 20°
θ

A 1.75 in. dia. brass aperture was at the flare aperture in Run 5. The aperture had no measurable effect on the 0° response as is predicted by Eq. 9. $V_5(\theta)$ is shown by crosses in Fig. 20. The solid curve in Fig. 20 is the derived function $I_A(\theta)$. As was the case for Run 1, the theoretical curve is somewhat broader than the experimental one for small angles. At 14°, where $I_A(\theta)$ goes to zero, the radiometer signal has fallen only by a factor of 50 from the 0° signal. Light which is reflected by the aperture back into the cone is probably the chief cause for the signal being so strong at large angles. It was predicted that these types of reflections would occur for $8^{\circ} < \theta < 12.5^{\circ}$ and $18^{\circ} < \theta < 21^{\circ}$. There is no indication in Fig. 20 of reflections for the lower range; however, an obvious bumb occurs for $16^{\circ} < \theta < 20^{\circ}$ which corresponds closely to the upper range.

When the objective lens was placed over the brass aperture in Run 6, the angular distribution was sharpened considerably. Furthermore, the effect of aperture reflections was made very pronounced. The circles in Fig. 21 show $V_6(\theta)$. Two large bumbs occur at $9^{\circ} < \theta < 12^{\circ}$ and $16^{\circ} < \theta < 19^{\circ}$ which correspond to the predicted ranges for aperture reflections. A third bumb occurs for $23^{\circ} < \theta < 27^{\circ}$ which is left unexplained.

In Run 7 the brass aperture was covered with a .125 in. layer of Apiezon, a black vacuum sealing compound. It was hoped that the compound would be optical black for the far infrared and absorb the incident light thereby eliminating aperture reflections. The crosses in Fig. 21 show the results of Run 7. The first two bumbs that

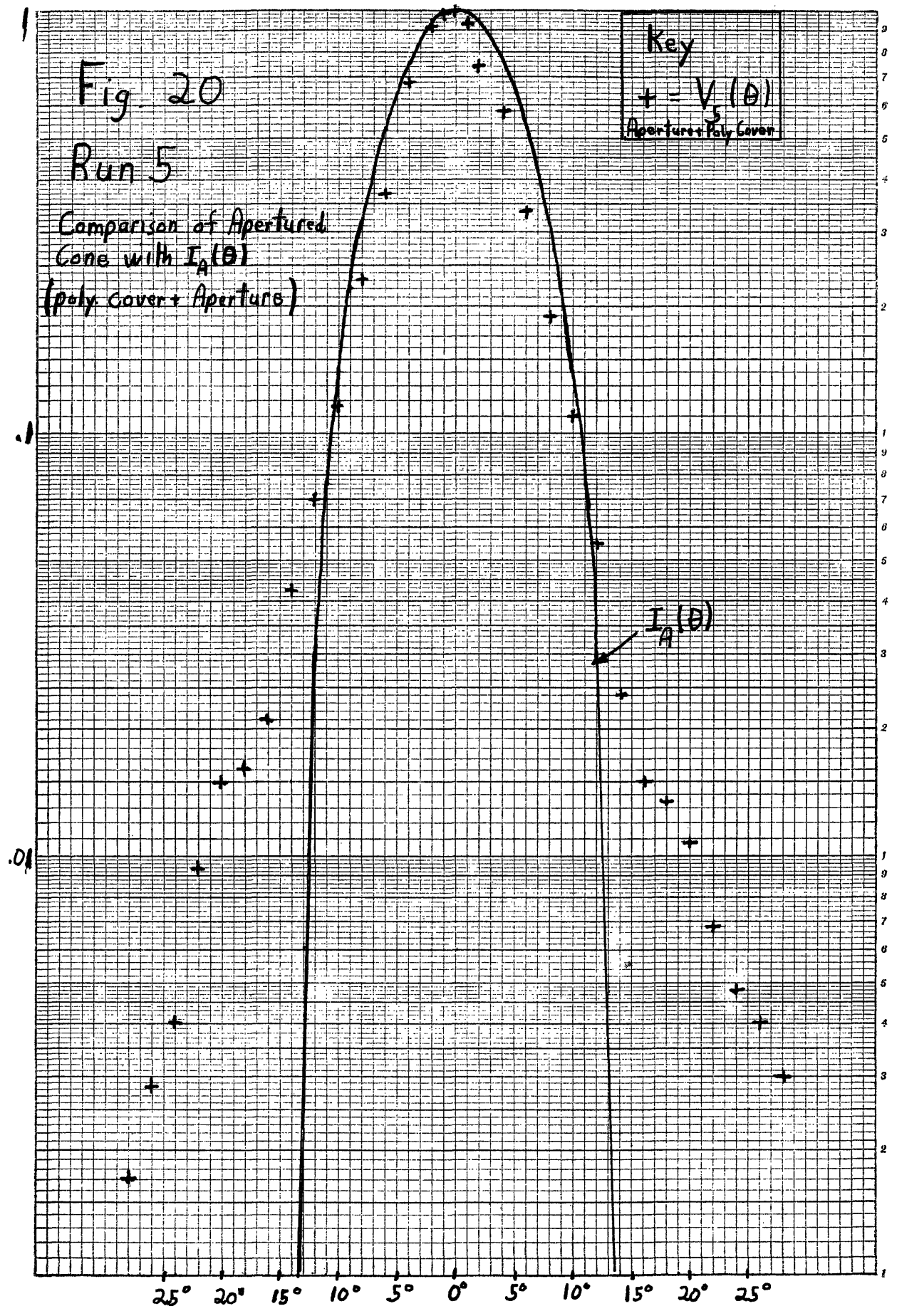
Fig. 20
Run 5
Comparison of Apertured Cone with $I_A(\theta)$
(poly cover + Aperture)
Key
+ = $V_s(\theta)$
Aperture + Poly Cover
$I_A(\theta)$
1
.1
.01
25° 20° 15° 10° 5° 0° 5° 10° 15° 20° 25°

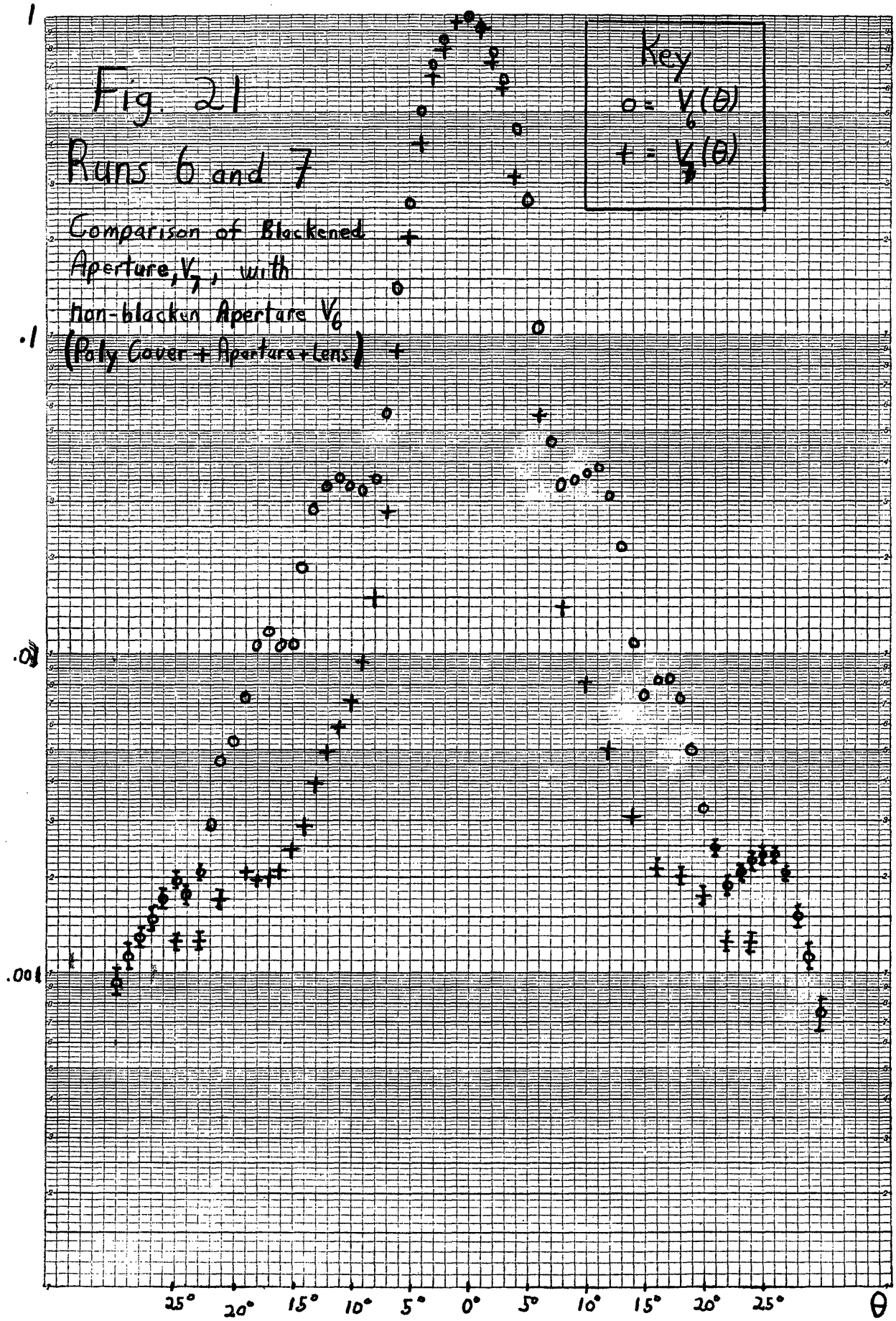
Fig. 21
Runs 6 and 7
Comparison of Blackened Aperture, V_7, with Non-blacken Aperture V_6
(Poly Cover + Aperture + Lens)
Key
o = $V_6(\theta)$
+ = $V_7(\theta)$
1
.1
.01
.001
25°
20°
15°
10°
5°
0°
5°
10°
15°
20°
25°
θ

appeared in Run 6 completely disappeared indicating that the Apiezon did reduce the reflections. The bumb for $23^{\circ} < \theta < 27^{\circ}$ was somewhat reduced but did not completely disappear, leading one to believe that it is caused by something other than aperture reflections.

In Runs 8, 9, and 10 filters were used in conjunction with the lens and aperture. The filters were held above the lens by another 1.75 in. dia. brass aperture. In Run 8 filter A was placed .5 in. above the lens, and the data is shown by circles in Fig. 22. Filter B was placed 1 in. above the lens in Run 9. $V_9(\theta)$ is shown by "x's" in Fig. 22. In Run 10 filter C was .75 in. above the lens, and the results are indicated by crosses in Fig. 22. The arrangement of apertures, lens, and filter in Run 9 was the same as the SR-2 arrangement in the 1969 balloon-borne radiometer, and the arrangement for Run 10 duplicated the SR-3 arrangement. Note that the angular distributions for the three filters are very similar. The bumbs in the distributions are probably due to aperture reflections.

Let the antenna function of the radiometer be defined as the angular response multiplied by $\sin\theta$. Fig. 23 shows the antenna function for Run 7, and Fig. 24 shows it for Run 10. The integrals of the antenna functions normalized to one for $\theta = \pi/2$ are given in Figs. 25 and 26 for Run 7 and Run 10 respectively.

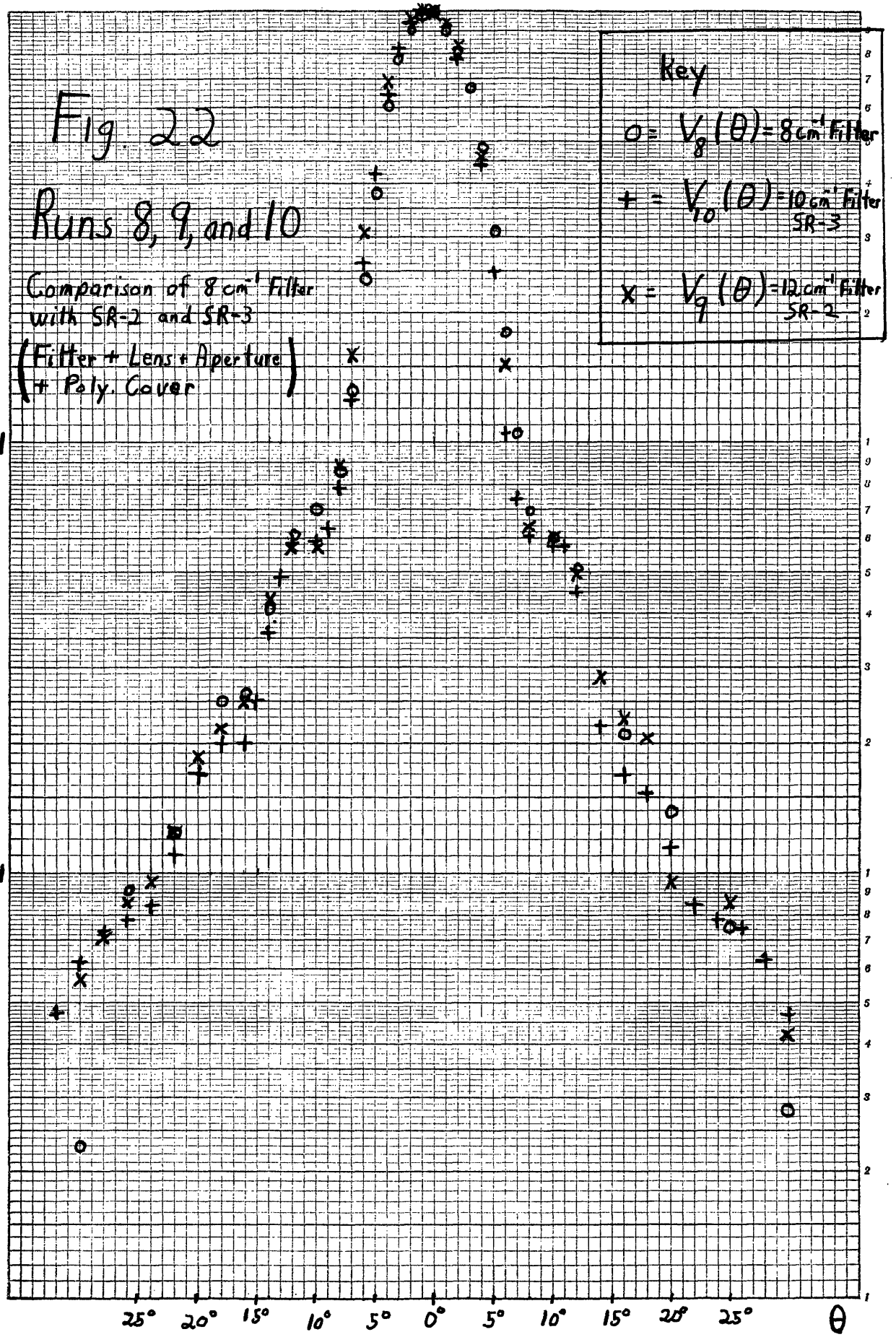
Fig. 22
Runs 8, 9, and 10
Comparison of 8 cm⁻¹ Filter with SR-2 and SR-3
(Filter + Lens + Aperture + Poly. Cover)
Key
o = V8(θ) = 8 cm⁻¹ Filter
+ = V10(θ) = 10 cm⁻¹ Filter SR-3
x = V9(θ) = 12 cm⁻¹ Filter SR-2
1
.1
.01
25° 20° 15° 10° 5° 0° 5° 10° 15° 20° 25° θ

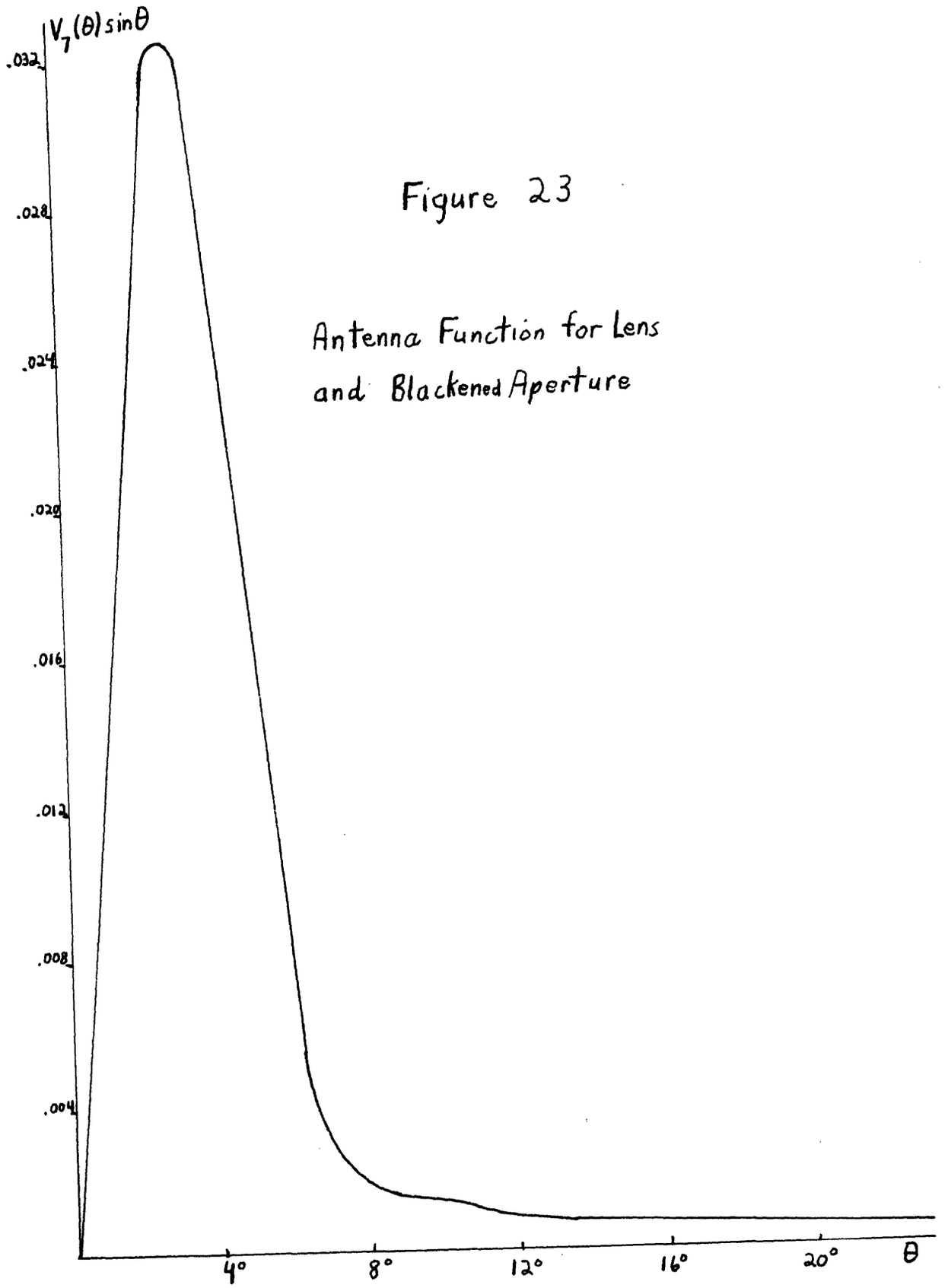

Figure 23

Antenna Function for Lens and Blackened Aperture

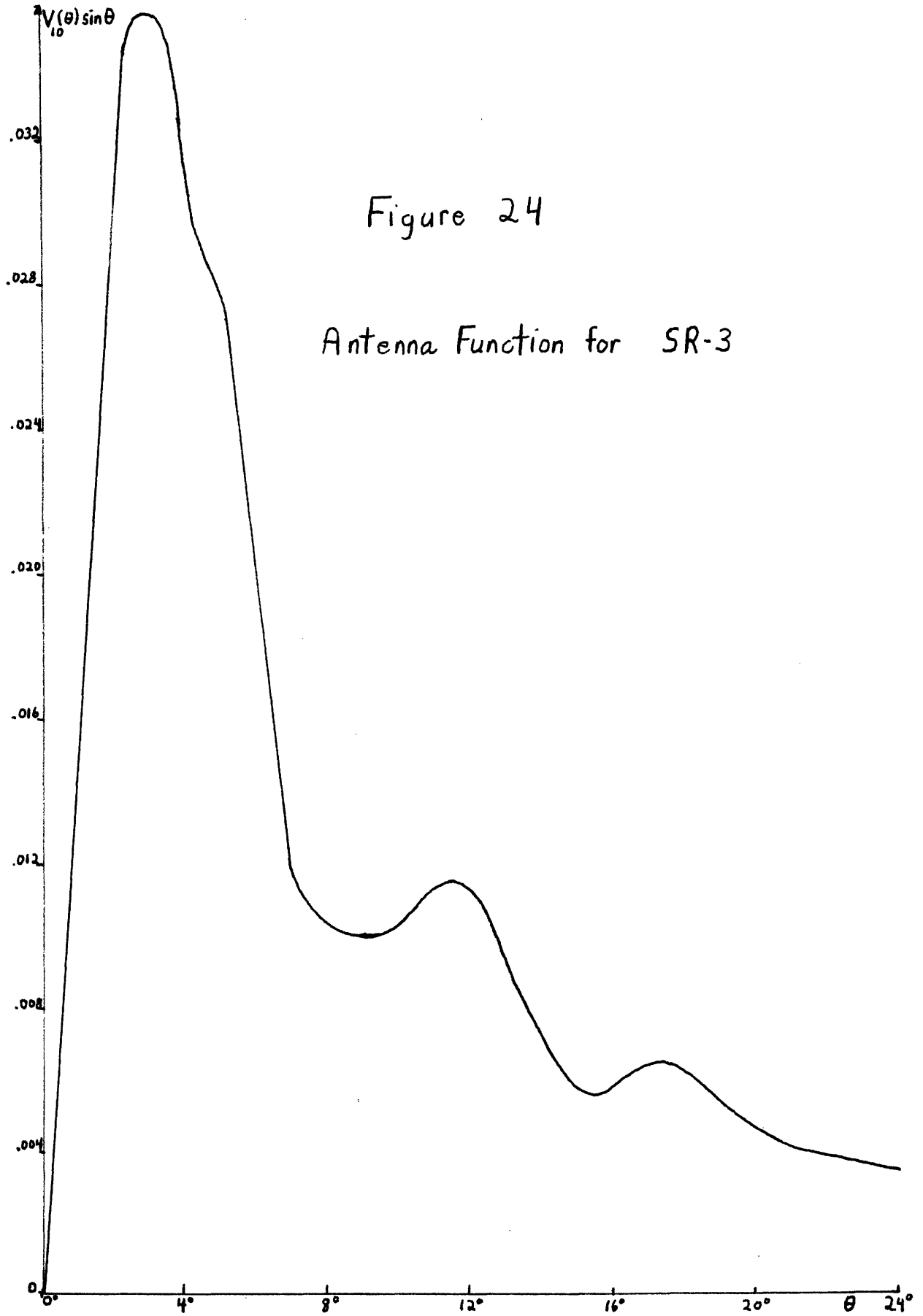

Figure 24

Antenna Function for SR-3

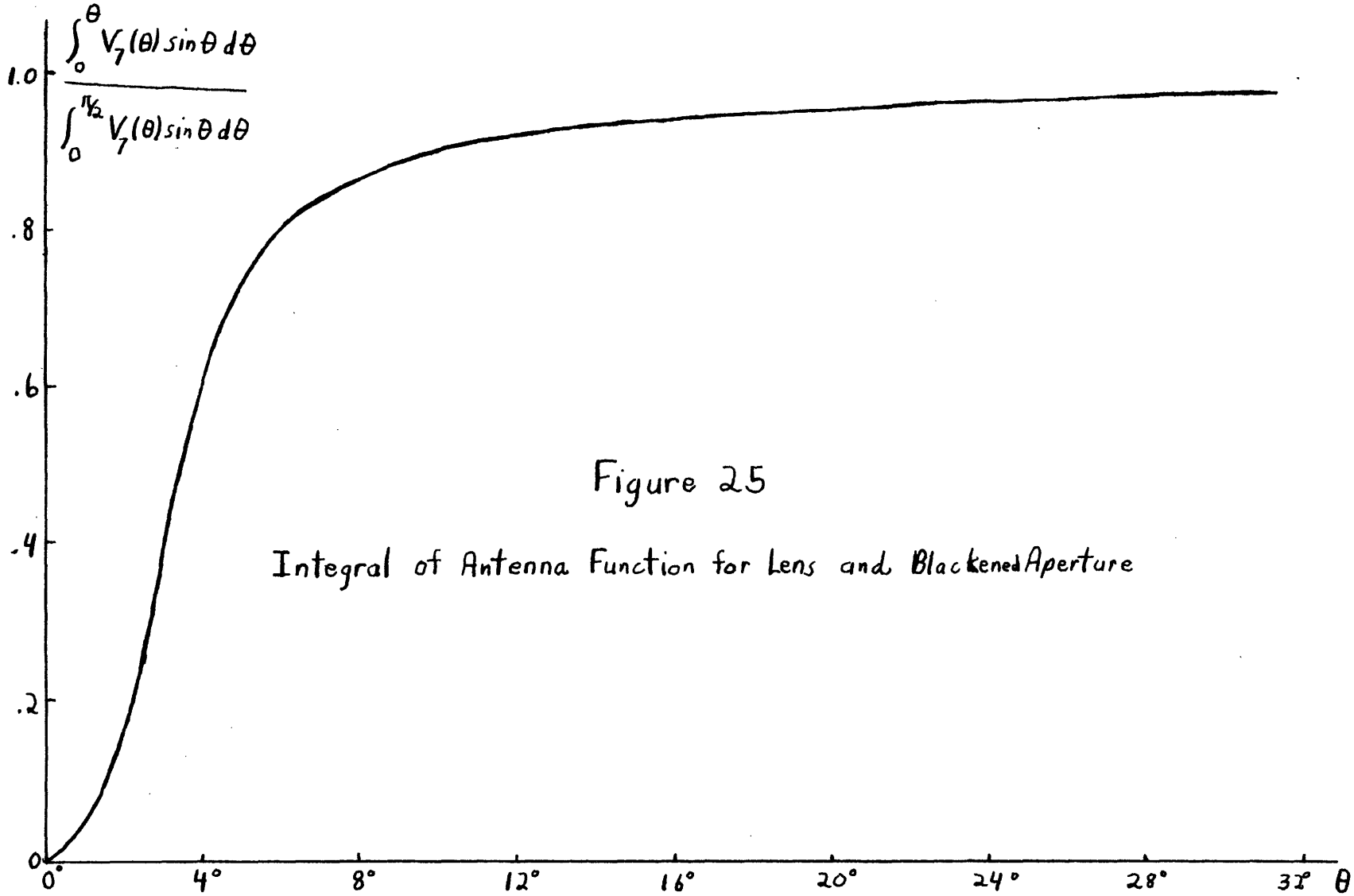

Figure 25

Integral of Antenna Function for Lens and Blackened Aperture

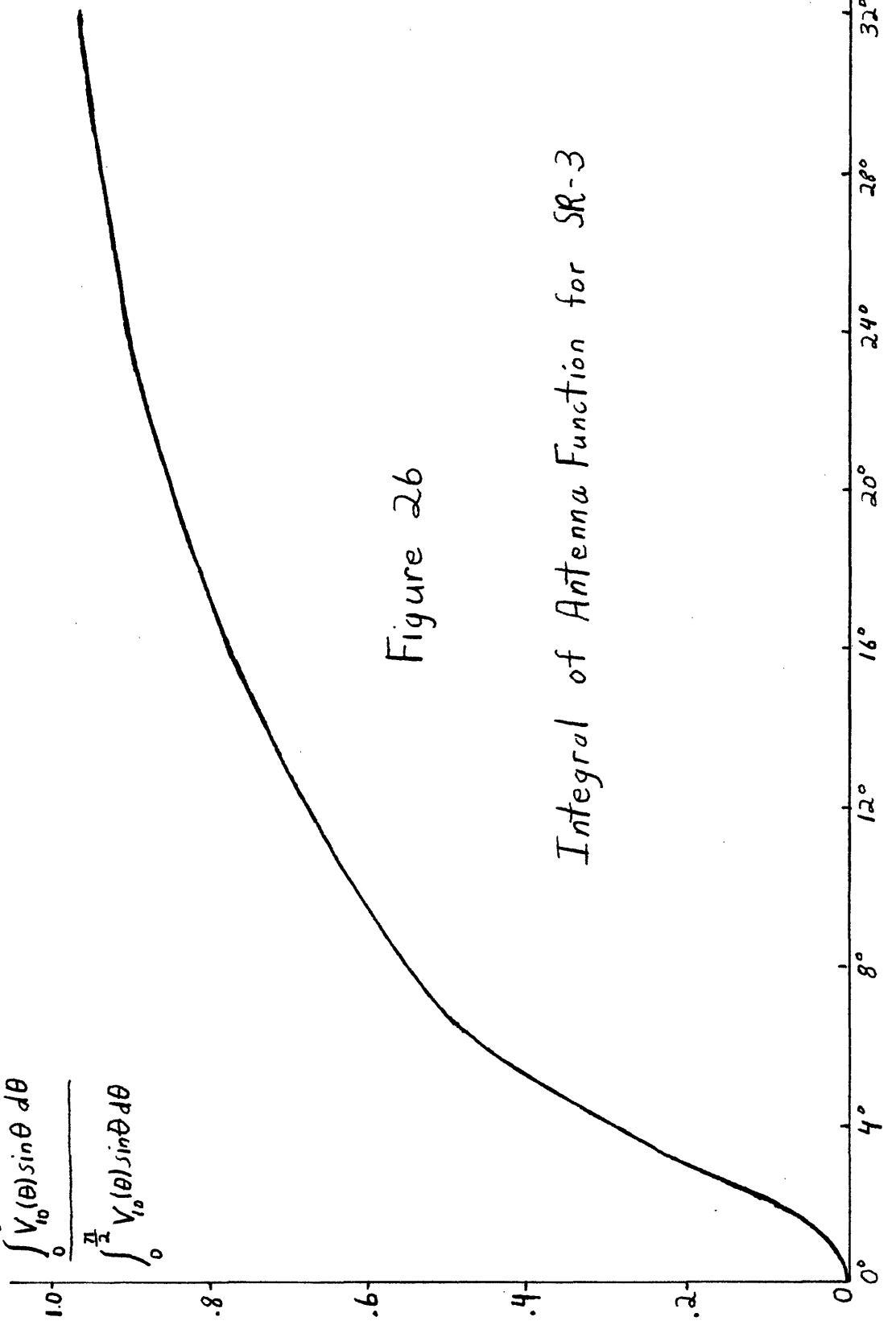

Figure 26

Integral of Antenna Function for SR-3

Conclusions

After comparing the results of the experiment with the theory, several basic conclusions can be made. First, the intrinsic angular distribution of the cone can be well represented by the geometric angular distribution with the addition of a weak tail at large angles resulting from diffraction. Furthermore, it was shown that the objective lens does considerably sharpen the angular distribution as was expected. This is useful to know because it is desirable to have a sharp distribution for the balloon experiment. The aperture had the opposite effect on the distribution. It resulted in broadening the distribution because of reflections from it. To achieve a sharp angular response, the aperture and anything else which might reflect light back into the cone should be made of a absorbing material if possible. Finally, it was found that the SR-2 and SR-3 arrangements had nearly the same angular distribution. The importance of this is that it rules out one possible explanation for the ratio anomaly measured in the 1969 balloon experiment.

Appendix 1

Stratton[11] derives the following approximations for the reflection coefficients of a metal. These expressions are correct to the second order of x.

$$R_p \approx \frac{2\cos^2\gamma - 2x\cos\gamma + x^2}{2\cos^2\gamma + 2x\cos\gamma + x^2} \qquad \text{Eq 13}$$

$$R_s \approx 1 - 2x\cos\gamma \quad , \qquad \text{Eq 14}$$

where $x = (2\epsilon_0\omega\rho)^{\frac{1}{2}}$, ω is the angular frequency of the light, ρ is the resistivity of the metal, and γ is the angle of incidence. The s and p refer respectively to the polarizations perpendicular and parallel to the plane of incidence. For the highest frequency accepted by the radiometer, the value of x for gold is 1.3×10^{-3} at room temperature and 1.1×10^{-4} for temperatures around 10°K. Both values are such that $x \ll \cos\gamma$ except for $\gamma \approx 90^{\circ}$ which is an isolated point. Since $x/\cos\gamma \ll 1$, R_p and R_s can be well approximated by

$$R_p \approx 1 - 2x/\cos\gamma \approx e^{-2x/\cos\gamma} \qquad \text{Eq. 15}$$

$$R_s \approx e^{-2x\cos\gamma} \quad . \qquad \text{Eq 16}$$

Axial rays entering a light pipe of length H and diameter d at an incident angle θ with respect to the pipe's axis will make $(H\tan\theta)/d$ reflections in the pipe. The rays will make an incident angle with respect to the pipe's walls of $\gamma = 90^{\circ} - \theta$. The total amount of transmitted radiation is then given by

$$T_p \approx \exp\left[(-2x/\sin\theta)(H\tan\theta)/d\right] \qquad \text{Eq. 17}$$

$$T_s \approx \exp\left[(-2x\sin\theta)(H\tan\theta)/d\right]. \qquad \text{Eq. 18}$$

The light pipe in this experiment can be divided into two regions, the top 3 inches at room temperature above the liquid helium and the bottom 12 inches at liquid helium temperature. The total transmission of the light pipe is equal to the product of the transmissions of the two regions. Putting the appropriate values in for H, d, and x, one obtains

$$T_p \approx e^{-.02/\cos\theta} \qquad \text{Eq. 19}$$

$$T_s \approx e^{-.02\sin^2\theta/\cos\theta}. \qquad \text{Eq. 20}$$

A ray of light just making it thru the apex aperture of the cone will be reflected by the brass cone leading into the light pipe in such a manner that it will enter the light pipe at $\theta = 22^\circ$. All other rays enter the light pipe at smaller angles. This was determined by simple ray tracing. Therefore , minimum transmission occurs for $\theta = 22^\circ$. Letting $\theta = 22^\circ$, one finds that $T_p = .98$ and $T_s = .997$. Thus the transmission of the light pipe varies by no more than 2% as a function of incident angle.

Appendix 2

Fig. 27 shows two circles of radii r and $R' = R\cos\frac{1}{2}\theta$. Their centers are separated by a distance of $d = L\sin\theta$. The overlap area A of the two circles is easily found. From the geometry of Fig. 27,

$$X(R',r,d) \equiv \overline{P_1P_0} = (d^2+R'^2-r^2)/2d . \qquad \text{Eq. 21}$$

Dividing area A into two areas, A_1 and A_2, one finds

$$F_1(R',r,d) \equiv A_1 = \int_{X(R',r,d)}^{R'} dx\,(2\sqrt{R'^2-x^2}) \qquad \text{Eq. 22}$$

$$F_2(R',r,d) \equiv A_2 = \int_{d-r}^{X(R',r,d)} dx\,(2\sqrt{r^2-(x-d)^2}) . \qquad \text{Eq. 23}$$

Substituting $y = d - x$ into Eq. 23 one obtains

$$F_2(R',r,d) = -\int_{r}^{d-X(R',r,d)} dy\,(2\sqrt{r^2-y^2}) , \qquad \text{Eq. 24}$$

and using the following relationships

$$d - X(r,R',d) = X(R',r,d) \qquad \text{Eq. 25}$$

$$F_2(r,R',d) = -\int_{R'}^{d-X(r,R',d)} dy\,(2\sqrt{R'^2-y^2}) , \qquad \text{Eq. 26}$$

one finally obtains

$$F_2(r,R',d) = F_1(R',r,d) . \qquad \text{Eq. 27}$$

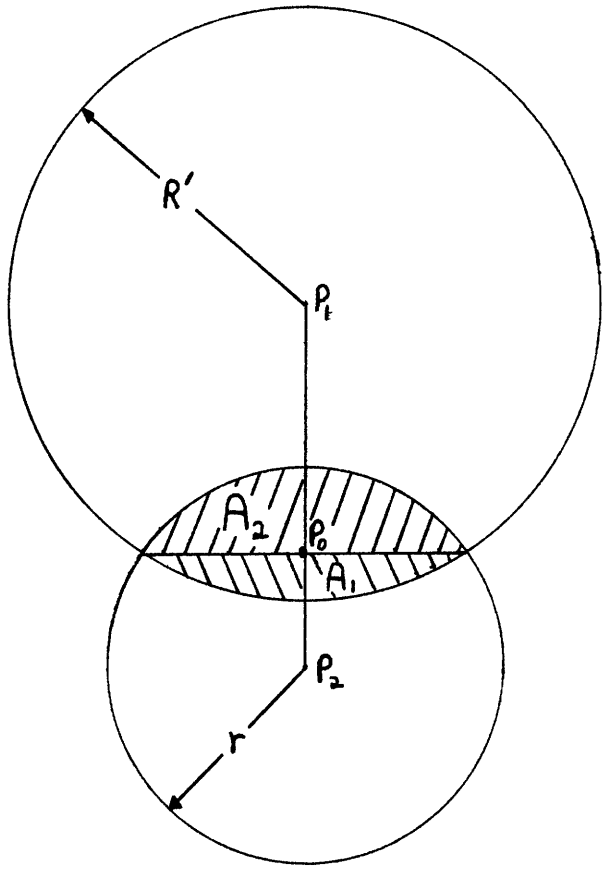

Figure 27

Intersection of Reference Sphere and Incident Light

Therefore,

$$F(R', r, d) \equiv A = F_2(R', r, d) + F_2(r, R', d). \quad \text{Eq. 28}$$

The result of the integration gives

$$F_2(R', r, d) = \frac{\pi r^2}{2} - X(r, R', d)\left[r^2 - (X(r, R', d))^2\right]^{\frac{1}{2}} - r^2 \sin^{-1}\left(\frac{X(r, R', d)}{r}\right) \quad \text{Eq 29}$$

The above expression for F(R',r,d) holds for $R'-r \leq d \leq R'+r$. For $d < R'-r$ the two circles completely overlap and $F(R',r,d) = \pi r^2$. For $d > R'+r$ the two circles do not intesect and $F(R',r,d) = 0$.

Appendix 3

Fig. 28 shows the intersection of the solid angle distribution $\Omega_\theta(t')$ with the reference sphere. Refering to Eqs. 1 and 7, one has

$$\Omega_\theta(t') = \begin{cases} 1 & t' \le \cos^{\frac{1}{2}}\theta \\ 3-(2t'/\cos^{\frac{1}{2}}\theta) & \cos^{\frac{1}{2}}\theta < t' < 1.5\cos^{\frac{1}{2}}\theta \\ 0 & t' \ge 1.5\cos^{\frac{1}{2}}\theta \end{cases}$$

Eq. 30

Let $A'(\theta)$ equal the overlap area of the circle of radius $\cos^{\frac{1}{2}}\theta$ with the reference sphere. Then from Appendix 2 one has

$$A'(\theta) = F(\cos^{\frac{1}{2}}\theta, r, \overline{P_1P_2}) \qquad \text{Eq. 31}$$

Refering to Fig. 12, one sees that $\overline{P_1P_2} = 8.1\sin\theta$. $\Omega_\theta(t') = 1$ everywhere in $A'(\theta)$. The brightness distribution over $A'(\theta)$ can not be easily expressed in terms of the prime coordinates. To avoid having to do this, the following approximation is made. Let the brightness distribution be replaced by its average value $\bar{B}(\theta)$ over $A'(\theta)$. Refering to Fig. 12 and Eq. 10, $\bar{B}(\theta)$ can be written as

$$\bar{B}(\theta) = \int_{A'(\theta)} (1-.08z)\,dA' \Big/ A'(\theta)$$

$$\approx \int_{11.5\sin\theta'-r}^{b} (1-.08|z|)\,dz \Big/ (b-11.5\sin\theta'+r) \qquad \text{Eq 32}$$

where b represents the maximum value of z in the region $A'(\theta)$. The above approximation for $\bar{B}(\theta)$ is within 1% of its actual value. Therefore, the total intensity of light incident on $A'(\theta)$ is

$$I^{A'}(\theta) = \int_{A'(\theta)} \Omega_\theta(t')\,\bar{B}(\theta)\,dA' = \bar{B}(\theta)A'(\theta) \qquad \text{Eq. 33}$$

Fig. 28 Intersection of $\Omega_\theta(t')$ with Reference Sphere

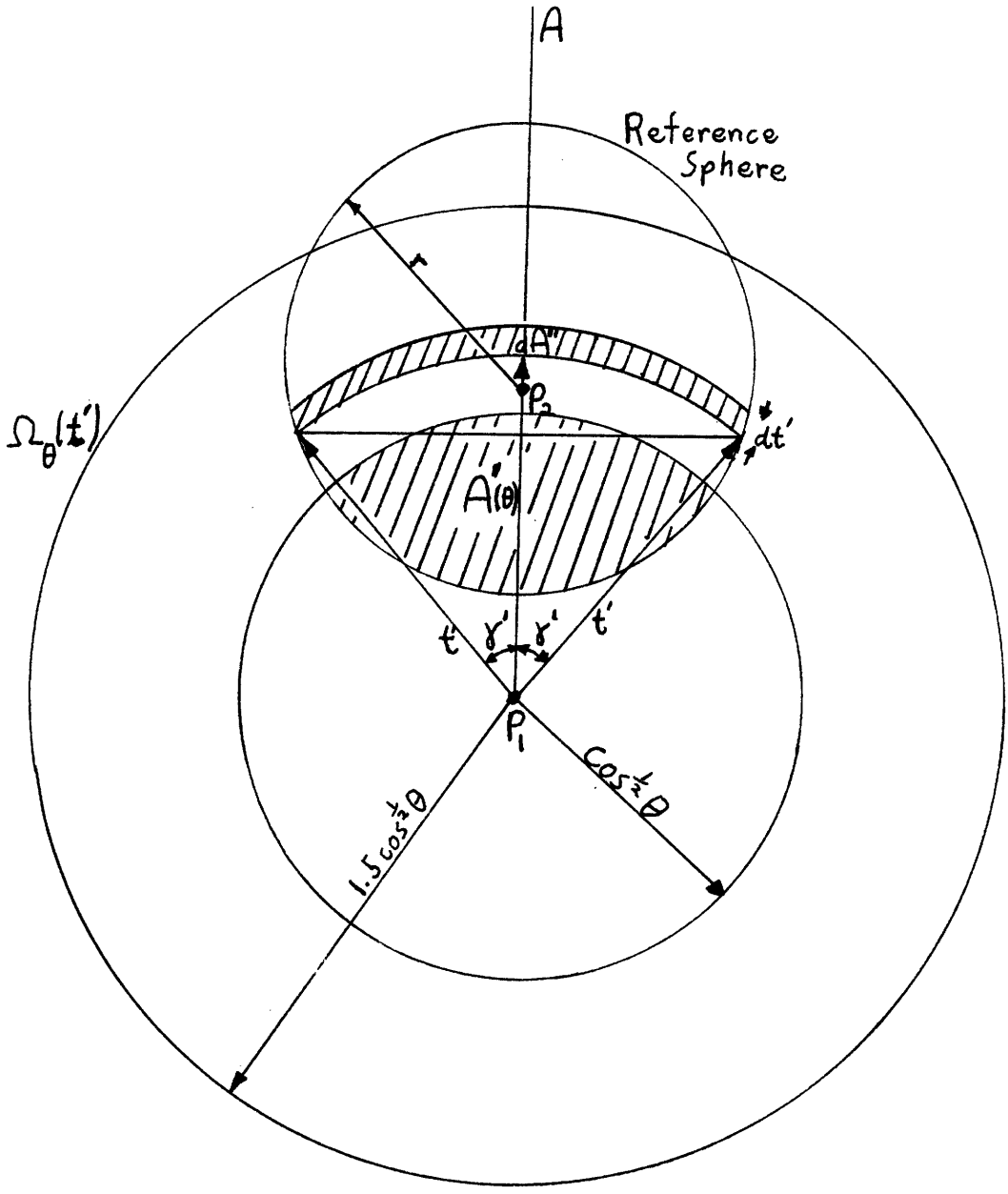

Let $A''(\theta)$ represent the overlap area of the circle of radius $1.5\cos^{\frac{1}{2}}\theta$ with the reference sphere minus the area $A'(\theta)$. Furthermore, let dA" be an area element in $A''(\theta)$ such that

$$dA'' = 2\gamma' t' dt' \,, \qquad \text{Eq. 34}$$

where, refering to Fig. 26,

$$\gamma' = \cos^{-1}\left(\frac{\overline{P_1P_0}}{t'}\right) \qquad \text{Eq. 35}$$

$$\overline{P_1P_0} = (t'^2 - r^2 + \overline{P_1P_2}^2)/2\overline{P_1P_2} \,. \qquad \text{Eq. 36}$$

In the region $A''(\theta)$, $\Omega_\theta(t')$ is given by the second expression in Eq. 30. The brightness distribution is not constant over dA" because B(z) is not symmetric about P_1 except for $\theta = 0^\circ$. However, B(z) varies only a few per cent over dA", and it can be very well approximated by its value along line A in Fig. 28. Therefore, let the brightness of dA" be given by

$$\bar{B}_\theta(t') = 1 - .08(t' + 3.4\sin\theta') \qquad \text{Eq. 37}$$

The total intensity of light impinging on $A''(\theta)$ is given by

$$I^{A''}(\theta) = \int_{A''(\theta)} \bar{B}_\theta(t')\,\Omega_\theta(t')\,dA''$$

$$= \int_c^{1.5\cos^{\frac{1}{2}}\theta} (3 - 2t'\cos^{-\frac{1}{2}}\theta)[1 - .08(t' + 3.4\sin\theta')](2\gamma' t' dt') \qquad \text{Eq. 38}$$

where c is the lower limit of integration and is given by

$$c = \begin{cases} \cos^{\frac{1}{2}}\theta & 3.4\sin\theta' - r < \cos^{\frac{1}{2}}\theta \\ 3.4\sin\theta' - r & \text{otherwise} \end{cases} \qquad \text{Eq. 39}$$

The total intensity equals

$$I(\theta) = I^{A'}(\theta) + I^{A''}(\theta) \qquad \text{Eq. 40}$$

These integrals were done numerically on a IBM 360, and the results are shown in Fig. 13.

References

1 D. Muehlner and R. Weiss, Phys. Rev. Letters 24, 742 (1970).

2 R. Cano and M. Mattioli, Infrared Phys. 7, 25 (1967).

3. R. Papoular, Infrared Phys. 4, 137 (1964).

4. B. V. Rollin, Proc. Phys. Soc. (London) 76, 802 (1960).

5. M. A. Kinch and B. V. Rollin, Brit. J. Appl. Phys. 14, 672 (1963).

6. D. Muehlner, A Measurement of the Background Radiation in the Far Infrared, PhD. Thesis, M.I.T., (1970).

7. D. E. Williamson, J. Opt. Soc. Am. 42, 712 (1952).

8. W. White, Infrared Phys. 5, 179 (1965).

9. R. Ulrich, Infrared Phys. 7, 65 (1967).

10. M. G. Schorr and F. J. Beck, Jr., J. Appl. Phys. 21, 795 (1950).

11. J. A. Stratton, Electromagnetic Theory, (McGraw-Hill, New York, 1941) p. 505.